

Coiled Tubing Pipe Mechanics

Final Report

(March 1995-August 1998)

Prepared by:

Ken Newman

CTES, L.C.
9870 Pozo Lane
Conroe, TX 77303
www.ctes.com

Prepared For:
GAS RESEARCH INSTITUTE
Contract No. 6011

GRI Project Manager
Steve Wolhart
E&P Research Deployment

April 2002

LEGAL NOTICE

This report was prepared by CTES, L.C. as an account of work sponsored by Gas Technology Institute (GTI). Neither GTI, members of GTI, nor any person acting on behalf of either:

- a. MAKES ANY WARRANTY OR REPRESENTATION, EXPRESS OR IMPLIED WITH RESPECT TO THE ACCURACY, COMPLETENESS, OR USEFULNESS OF THE INFORMATION CONTAINED IN THIS REPORT, OR THAT THE USE OF ANY INFORMATION, APPARATUS, METHOD, OR PROCESS DISCLOSED IN THIS REPORT MAY NOT INFRINGE PRIVATELY OWNED RIGHTS, OR
- b. ASSUMES ANY LIABILITY WITH RESPECT TO THE USE OF, OR FOR ANY AND ALL DAMAGES RESULTING FROM THE USE OF, ANY INFORMATION, APPARATUS, METHOD, OR PROCESS DISCLOSED IN THIS REPORT.
- c. REFERENCE TO TRADE NAMES OR SPECIFIC COMMERCIAL PRODUCTS, COMMODITIES, OR SERVICES IN THIS REPORT DOES NOT REPRESENT OR CONSTITUTE AN ENDORCEMENT, RECOMMENDATION, OR FAVORING BY GTI OR ITS CONTRACTORS OF THE SPECIFIC COMMERCIAL PRODUCT, COMMODITY, OR SERVICE.

Public reporting burden for this collection of information is estimated to average 1 hour per response, including the time for reviewing instructions, searching existing data sources, gathering and maintaining the data needed, and completing and reviewing the collection of information. Send comments regarding this burden estimate or any other aspect of this collection of information including suggestions for reducing this burden to Washington Headquarters Services, Directorate for Information Operations and Reports, 1215 Jefferson Davis Highway, Suite 1204, Arlington, VA 22202-4302, and to the Office of Management and Budget, Paperwork Reduction Project (0704-0188), Washington, D.C. 20503.

1. AGENCY USE ONLY (Leave blank)		2. REPORT DATE February 26, 2002	3. REPORT TYPE AND DATES COVERED March 1995 – August 1996	
4. TITLE AND SUBTITLE Coiled Tubing Pipe Mechanics			5. FUNDING NUMBERS GTI contract no. 5095-210-3573	
6. AUTHOR(S) Ken Newman Udaya B. Sathuvalli		M. Scott Quigley Steve Tipton		
7. PERFORMING ORGANIZATION NAME(S) AND ADDRESS(ES) CTES, L.C. 9870 Pozos Lane, Conroe, TX 77303			8. PERFORMING ORGANIZATION REPORT NUMBER GRI-02/0058	
9. SPONSORING/MONITORING AGENCY NAME(S) AND ADDRESS(ES) GTI 1700 S. Mount Prospect Rd. Des Plaines, IL 60018			10. SPONSORING/MONITORING AGENCY REPORT NUMBER	
11. SUPPLEMENTARY NOTES				
12a. DISTRIBUTION/AVAILABILITY STATEMENT			12b. DISTRIBUTION CODE	
13. ABSTRACT (Maximum 200 words) Coiled Tubing (CT) experiences 6 cycles of plastic deformation due to bending for each trip into and out of a well. Each cycle alters the mechanical properties of the CT material, thereby complicating the problem of determining safe operating limits. This project conducted experiments to determine effects of strain-controlled cycling and internal pressure on the material properties of CT. Results from these experiments show that the yield strength of CT decreases by as much as 15% in the first few cycles, and gradually decreases during subsequent cycles. Moreover, the relationship of stress to strain is highly nonlinear after the first strain cycle. The tests clearly show that ballooning occurs only with internal pressure and is proportional to the axial strain on the CT. These results are conservative since the distribution of strain in the CT cross section is not uniform. Residual stresses in CT due to bending are significant enough to affect the accuracy of operating limits calculated using the incipient yield criteria. An alternative method for calculating limit states based on a probabilistic approach that accounts for effects of cyclic loading is proposed.				
14. SUBJECT TERMS Coiled tubing, pipe mechanics			15. NUMBER OF PAGES 62	
			16. PRICE CODE	
17. SECURITY CLASSIFICATION OF REPORT Unclassified	18. SECURITY CLASSIFICATION OF THIS PAGE Unclassified	19. SECURITY CLASSIFICATION OF ABSTRACT Unclassified	20. LIMITATION OF ABSTRACT	

Research Summary

Title	Coiled Tubing Pipe Mechanics
Contractor(s)	CTES, L.C. - GTI Contract Number 5095-210-3573
Principal Investor(s)	CTES, L.C.
Report Type	Final Report #GRI-02/0058
Report Period	March 1995 – August 1998

Project Objectives

- A. Determine effects of strain-controlled cycling and internal pressure on the material properties of CT.
- B. Develop an analytical model for the material properties behavior observed in (A).
- C. Propose an alternative to the limit state criteria for CT based on incipient yield.
- D. Implement the analytical model and new limit state criteria in software designed for predicting CT mechanical behavior.

Technical Perspective

Coiled Tubing (CT) experiences 6 cycles of plastic deformation due to bending for each trip into and out of a well. Each cycle introduces residual stresses and alters the mechanical properties of the CT material. Moreover, pressure inside the CT during plastic deformation causes ballooning of the CT diameter and a corresponding reduction in wall thickness. These effects complicate the problem of determining safe operating limits for the CT. The current method of calculating operating limits uses the von Mises incipient yield criteria which ignores residual stresses and changes in material properties due to cyclic strain. An alternative method for calculating limit states based on a probabilistic approach that accounts for effects of cyclic loading is needed.

Technical Approach

Cyclic strain tests (CST) in an axial tension/compression machine were performed with samples of 1.5-in and 2.0-in CT. The strains were large enough in each load cycle to plastically deform the sample. Some of the samples were pressurized to determine the triaxial stress/strain relationship

and its effects on ballooning. Each CST provided accurate measurements of axial force on the CT sample and axial strain. Hoop strain and pressure were also measured during pressurized tests. These data were analyzed in the form of the stress versus strain curves.

Results

Due to a shortfall of member funding, GRI could only provide enough funding for this project to partially meet the objectives stated above. The following summarizes the results for the work completed with the limited funding.

1. Cyclic loading changes the material properties of CT so that the elastic-perfectly-plastic model for the material behavior does not apply after the first cycle.
2. The yield strength of CT material decreases by approximately 15% with increasing strain cycles up to about 20 cycles.
3. The stress/strain curves exhibit self-similarity in the plastic region implying a power law relationship between stress and strain at different strain ranges.
4. Ballooning of the CT diameter only occurs during plastic deformation with internal pressure. The ballooning appears to be a linear function of the axial strain range.
5. The current method of defining CT limit states based on the von Mises incipient yield criterion is overly conservative because it neglects effects of residual stresses. An alternative criterion that accounts for effects of cyclic plastic deformation, residual stresses, and probability of failure is suggested.

Project Implications

CT is being used to service high-pressure gas wells. These services are much less expensive than services performed with a rig or snubbing unit. Better understanding of the pipe limits has been achieved through this research. This understanding, combined with other testing and research, has allowed CT to be used in wells with progressively higher wellhead pressures. When this project was initiated in 1995, it was unusual for CT operations to be performed in wells with wellhead pressures over 5,000 psi. CT operations in wells with pressures over 10,000 psi are now performed, with a huge savings to the natural gas industry. The understanding gained from this project was partially responsible for this increase.

MEMORANDUM

TO: Gas Technology Institute (GTI)
FROM: CTES, L.C.
SUBJECT: GTI Contract # 5095-210-3573
Report # GRI-02/0058

GTI is authorized to publish, have published, reproduce, have reproduced, distribute, have distributed, and sell or have sold on its behalf this copyrighted work. Permission for further reproduction must be obtained from the copyright owner.

(Signature of copyright owner or
authorized representative)

CTES, L.C. – Ken Newman
(Signature of copyright owner or
authorized representative)

April 1, 2002
Date

Table of Contents

Executive Summary	2
Introduction	3
Review of relevant literature	5
Loading events of coiled tubing	6
Residual stresses in coiled tubing	11
Cold working, Bauschinger effect and cyclic loading	14
Development of the cyclic strain test (CST)	16
Test apparatus, transducers & data acquisition system	18
Experimental data from CST	22
Rational for redefining CT limit states	33
Coiled Tubing Test Machine	37
Analysis of CTTM Fatigue Data	42
Conclusions	44
Recommendations	45
Nomenclature	46
References	48
Appendix A: CTTM Design Specifications	50
Appendix B: Surge tank calculations	51
Appendix C Log of CST 1-8	54

EXECUTIVE SUMMARY

Coiled Tubing (CT) experiences a high degree of cyclic loading in the field due to repeated bending on and off the reel and gooseneck. This results in significant deterioration of material properties. This project examines the problem of determining the operational limit states of CT in view of this cyclic loading. A series of experiments to determine the influence of strain controlled cycling and internal pressure on the material properties of CT were performed. The testing consisted of cycling a set of virgin CT samples between fixed strain limits in a universal testing machine with and without internal hydraulic pressure. The testing showed that the yield strength of CT decreases by as much as 15% in the first few cycles, and that the material behavior is significantly nonlinear. The tests also proved that ballooning occurs only when there is internal hydraulic pressure, and that diametral growth is proportional to the axial strain experienced by the pipe. The results from these tests are conservative since all parts of the CT cross section do not experience the same plastic strain when the CT is bent and straightened. Nevertheless, the tubing loses its elastic-plastic material properties after it is bent for the very first time.

The residual stresses present in the CT due to bending were calculated theoretically and it was shown that these stresses are significant enough to affect the incipient yield criteria as they are currently applied. Alternative schemes that account for cyclic loading and loading history of the CT string in the field are proposed for future consideration.

This research project has proven the following major points about the operational limits of coiled tubing in view of cyclic loading:

- Cyclic loading changes the material properties of CT so that the elastic-perfectly-plastic model for the material behavior does not apply after the first cycle.
- The yield strength of CT material decreases by approximately 15% with increasing strain cycles up to about 20 cycles.
- The stress/strain curves exhibit self-similarity in the plastic region implying a power law relationship between stress and strain at different strain ranges.
- Ballooning of the CT diameter only occurs during plastic deformation with internal pressure. The ballooning appears to be a linear function of the axial strain range.
- The current method of defining CT limit states based on the von Mises incipient yield criterion is overly conservative because it neglects effects of residual stresses. An alternative criterion that accounts for effects of cyclic plastic deformation, residual stresses, and probability of failure is suggested.

INTRODUCTION

The Coiled Tubing (CT) mechanics project was initiated in January 1996 at CTES by the Gas Technology Institute. The aim of the project was to define a new set of CT operating limits based on criteria other than "incipient yield". The new limit states would take into account the effects of residual stresses, property degradation due to cyclic loading and material anisotropy. This document describes the work done in this project through August 1996.

In contrast to other Oil Country Tubular Goods (OCTG), CT performance is dominated by two factors:

- a) severe cyclic loading and
- b) degradation of material properties during cyclic loading.

Therefore, a procedure that determines the operating "limit states" of CT must consider these two factors.

Presently, the burst, collapse and axial load operating limits for CT are established by using the von Mises incipient yield criterion [1]. This criterion has historically been used to calculate the limits for OCTG. The von Mises criterion calculates the tri-axial stresses (axial, circumferential, and radial) caused by the forces applied on the tubing due to

- axial force (tensile or compressive)
- internal and external hydraulic pressure
- bending (on the gooseneck or the reel and due to helical buckling).

The triaxial stresses caused by these externally applied forces and pressures are combined into a uniaxial equivalent stress, the von Mises stress, σ_{vme} . This combined stress, σ_{vme} , is then compared to the yield stress, σ_{yp} , determined from a uniaxial pull test on a sample of the CT. When σ_{vme} reaches σ_{yp} , it is assumed that the CT material will begin to yield [2]. This point of "incipient yield" is currently used by the CT industry to determine the burst, collapse, tensile and compressive limits for CT.

Because of the bending that occurs when CT is spooled on and off the reel and pulled over the gooseneck, the CT is plastically deformed before it enters a well. Also, the plastic bending and subsequent straightening introduce significant residual stresses in the CT. The current methods used to calculate limit states ignore these residual stresses. These residual stresses are a significant percentage of the yield stress of the material and initiate yielding earlier than predicted by the present method. The material used to make CT has a well-defined yield point in the axial direction for the first yield load applied. For subsequent loading cycles, the Bauschinger effect and work softening change σ_{yp} and make it less well defined. Also, σ_{yp} in the circumferential or hoop direction may not be the same as σ_{yp} in the axial direction [3].

This report contains a description of typical loading events that CT is subjected to. The residual stresses caused by plastic bending at the reel and the gooseneck are calculated by using a simple model. It is shown that these residual stresses are significant and must be considered in the calculation of CT operating limit states. The effect of cyclic loading on CT material properties is considered, and the methodology for Cyclic Strain Test (CST) for CT is presented. Finally, the results from the CSTs are discussed. The report ends with recommendations for future work on redefining the CT operating limit states.

REVIEW OF RELEVANT LITERATURE

The earliest work that determines the limit states of a tubular is reported in a German paper by Lode [4]. Lode subjected thin walled tubes of copper, nickel and steel to various combinations of internal hydrostatic pressure and uniaxial tension and devised a sensitive method to determine the effect of intermediate principal stresses on yielding. For an English translation of this work refer to the textbook by Slater [5]. In a set of classic experiments, Taylor and Quinney [6], subjected copper, mild steel and aluminum thin walled tubes to combined tension and torsion. Lode's work was repeated in part in 1945 by E. A. Davis of Westinghouse Research Laboratories [7], [8]]. Davis investigated the combined influence of tension and internal hydraulic pressure on the strength and ductility of thin walled tubes of low carbon steel. He studied the nature of tube failure for different ratios of axial to circumferential stress in the tube. It must be noted that these works were undertaken primarily to determine the limit states or the yield surfaces of ductile materials under multiaxial states of stress. Consequently, these studies did not include the effect of residual stresses and/or cyclic loading.

The earliest comprehensive study of cyclic loading from the point of view of view of low cycle fatigue is by Coffin [9]. Coffin's work considers the role of the Bauschinger effect and provides a very detailed review of work done on fatigue of ductile metals till 1954. For more details on Bauschinger effect consult the references cited in the section "Cold working, Bauschinger effect and cyclic loading."

LOADING EVENTS OF COILED TUBING

CT experiences stresses due to three kinds of loads:

- Bending (on the reel or on the gooseneck, or due to buckling inside the well) and straightening (when it comes off the reel or the gooseneck and in the injector head),
- direct tensile/compressive axial loading or unloading and
- internal and external hydraulic pressure.

In the absence of hydraulic pressure, the stresses induced are uniaxial along the axis of the tubing. Internal and/or external pressure creates a triaxial state of stress in the tubing. Figure 1 shows the three principal stresses in CT.

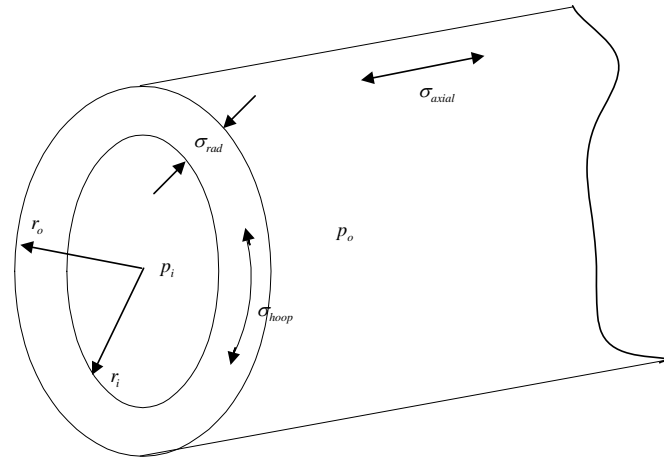


Figure 1 Principal stresses in CT

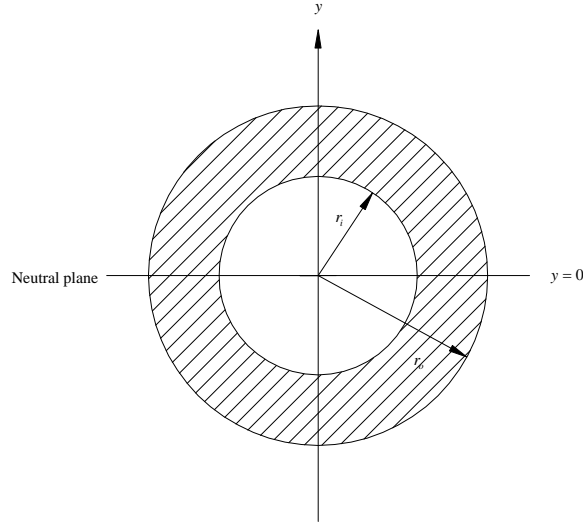


Figure 2 Cross section of CT

These principal stresses act along the axial, circumferential (or hoop), and radial directions. Internal and/or external hydraulic pressure create circumferential and radial stresses as shown in Figure 1. In general, the three principal stresses vary across the cross section. For example, in the absence of external pressure, with $p_i > p_o$ the hoop stress is maximum at the inside wall of the tubing and decreases outward. The axial stresses (though usually assumed constant) vary across the cross section when tubing is bent and straightened.

Consider the case when there is no internal or external pressure. When a length of CT is bent to a radius R_b and released, it returns to its initial straight position if $R_b \geq R_{b,y}$, or retains a residual radius of curvature R_r , if $R_b < R_{b,y}$. Here, $R_{b,y}$, the yield radius is defined as

Equation 1
$$R_{b,y} = \frac{d_o E}{2\sigma_{yp}}$$

Let a given length of CT be bent to a radius $R_b < R_{b,y}$ (where $R_{b,y}$ is the yield radius). Figure 3 shows the bending stress profile for this case obtained from elementary bending theory [10]. The fibers on one side of the neutral plane (see Figure 2) are in tension while those on the other are in compression. Upon completion of bending, the strain in the fibers is

Equation 2
$$\varepsilon_b(y) = \frac{y}{R_b}$$

where y is the distance of the fiber from the neutral plane, (which in this case happens to be the plane of bending). Assuming that the material is elastic perfectly plastic, the corresponding (axial) stress profile for the CT cross section is given by

Equation 3

$$\sigma_b(y) = \begin{cases} -\sigma_{yp}, & -r_o \leq y \leq -\varepsilon_y R_b, \\ \frac{Ey}{R}, & -\varepsilon_y R_b \leq y \leq \varepsilon_y R_b, \\ \sigma_{yp}, & \varepsilon_y R_b \leq y \leq r_o. \end{cases}$$

Let us divide the fibers in tension and compression into three sets of fibers

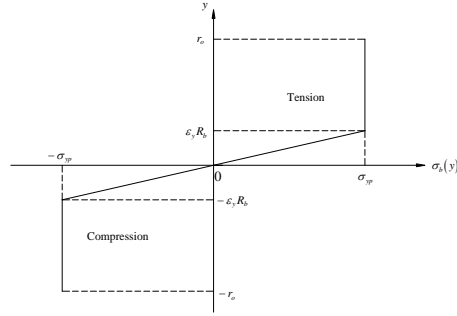


Figure 3 Bending stresses in CT

each, $\{T_1\}$, $\{T_2\}$, $\{T_3\}$ and $\{C_1\}$, $\{C_2\}$, $\{C_3\}$ and define the boundaries of each set of fibers as follows:

$$\{T_1\}: 0 \leq y \leq \varepsilon_y R_b,$$

$$\{T_2\}: \varepsilon_y R_b \leq y \leq 2\varepsilon_y R_b,$$

$$\{T_3\}: 2\varepsilon_y R_b \leq y \leq r_o,$$

$$\{C_1\}: 0 \leq y \leq -\varepsilon_y R_b,$$

$$\{C_2\}: -\varepsilon_y R_b \leq y \leq -2\varepsilon_y R_b,$$

$$\{C_3\}: -2\varepsilon_y R_b \leq y \leq -r_o$$

Fibers in tension,

Fibers in compression.

Table 1 shows the stresses and strains in each of these sets of fibers.

Table 1 Stresses and strains at the end of bending

Fiber set	Stress	Strain
$\{T_1\}$	$0 \leq \sigma_b = \frac{E}{R_b} y < \sigma_{yp}$	$0 \leq \varepsilon_3 \leq \varepsilon_y$
$\{T_2\}$	$\sigma_b = \sigma_{yp}$	$\varepsilon_y \leq \varepsilon_3 \leq 2\varepsilon_y$
$\{T_3\}$	$\sigma_b = \sigma_{yp}$	$2\varepsilon_y \leq \varepsilon_3 \leq \frac{d_o}{2R_b}$
$\{C_1\}$	$-\sigma_{yp} < \sigma_b = \frac{E}{R_b} y \leq 0$	$-\varepsilon_y \leq \varepsilon_3 \leq 0$
$\{C_2\}$	$\sigma_b = -\sigma_{yp}$	$-2\varepsilon_y \leq \varepsilon_3 \leq -\varepsilon_y$
$\{C_3\}$	$\sigma_b = -\sigma_{yp}$	$-\frac{d_o}{2R_b} \leq \varepsilon_3 \leq -2\varepsilon_y$

If the tubing is straightened, the strain in every fiber returns to zero. During straightening, each of the six sets of fibers behaves differently. All fibers in $\{T_1\}$ and $\{C_1\}$ return to zero stress. Fibers in $\{T_2\}$ and $\{C_2\}$ have finite stress less than the yield stress.

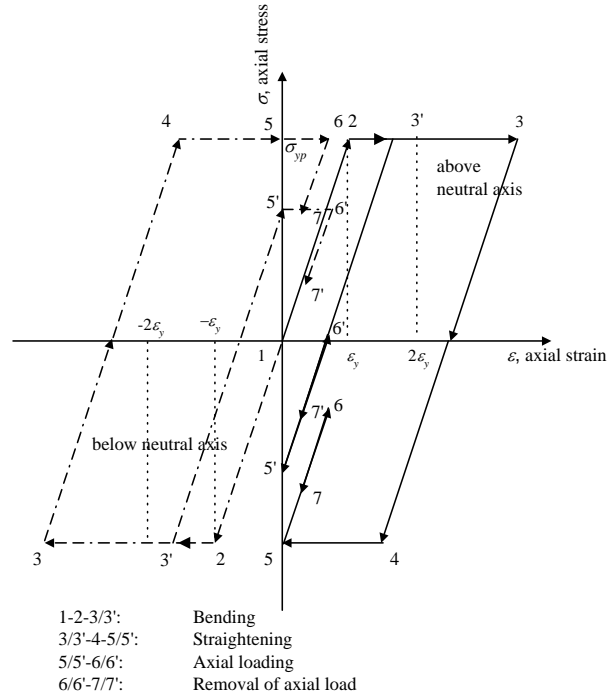


Figure 4 Loading diagram for elastic-perfectly-plastic CT

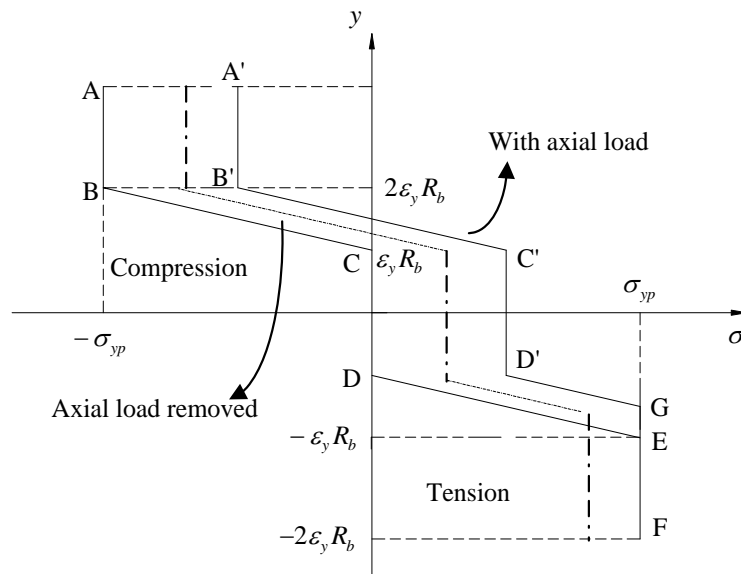


Figure 5 Stress profile in bent and straightened CT

Fibers in $\{T_3\}$ and $\{C_3\}$ have undergone strains greater than $|2\varepsilon_y|$ during bending. These fibers retain a residual stress equal to $|\sigma_{yp}|$ at the end of straightening. Figure 4 shows the stress profile at the end of straightening and Table 2 describes the stresses in each fiber set. Straightening interchanges the tension and compression regions. In addition, there is a stress free core in the center of the cross section. This stress free core is a characteristic feature plasticized beams that have been straightened [11].

Table 2 Stresses and strains at the end of straightening

Fiber set	Stress	Boundaries
$\{T_1\}$	0	$0 \leq y \leq \varepsilon_y R_b$
$\{T_2\}$	$-\frac{E}{R_b} y + \sigma_{yp}$	$\varepsilon_y R_b \leq y \leq 2\varepsilon_y R_b$
$\{T_3\}$	$-\sigma_{yp}$	$2\varepsilon_y R_b \leq y \leq r_o$
$\{C_1\}$	0	$0 \leq y \leq -\varepsilon_y R_b$
$\{C_2\}$	$-\frac{E}{R_b} y - \sigma_{yp}$	$-\varepsilon_y R_b \leq y \leq -2\varepsilon_y R_b$
$\{C_3\}$	σ_{yp}	$-2\varepsilon_y R_b \leq y \leq -r_o$

If a tensile axial load is applied to the bent and straightened CT, the stress profile shifts to the right and assumes the curve described by A'B'C'D'G as shown in Figure 5. The magnitude of the shift and the resulting axial strain can be calculated from elementary considerations involving force and moment balance [12], [13], [14], [15]]. Simultaneously, the various fibers in the cross section travel along the loading paths (5-6) shown in. Removal of axial load is elastic, i.e., all fibers in the CT unload along lines parallel to the elastic loading line (1-2 in Figure 4). Subsequent bending cycles essentially involve a repetition of the above events.

The simple model described above assumes that the CT material is elastic-perfectly-plastic. However, the Bauschinger effect observed in results from this study significantly alters the stress-strain behavior of the material. Moreover, the simple model assumes the CT cross section remains circular, a condition not found in actual practice. Repeated and severe bending of pipe causes ovality that does not vanish when pipe is straightened [16] This is also accompanied by a slight shift of the neutral axis and moment of inertia [17]. A complete mathematical description must consider these factors.

RESIDUAL STRESSES IN COILED TUBING

This section calculates the residual stresses in CT that is bent, released, straightened, and released again. The analysis assumes that

- i. the CT material is elastic perfectly plastic,
- ii. plane sections remain plane during bending, straightening, and release,
- iii. whenever the CT is released, the path of unloading of every fiber is elastic,
- iv. the axis of the CT lies in the neutral plane, and the neutral surface does not move and
- v. the bending radius is small enough for the elastic plastic boundary to have penetrated the inner radius of the CT¹, i.e., $R_b \leq r_i/\varepsilon_y$.

Assumption (i) is not strictly valid. A more complete model must relax this assumption and account for the change in material properties. When CT is bent, there is a slight shift of the neutral axis due to the Poisson effect². This effect may be neglected in the first analysis. However, the residual stresses calculated in this analysis indicate the order of magnitude of the expected stresses, and the method can be easily extended to account for the shift of the neutral surface.

Initial Bend

Upon completion of the initial bend, the strain and stress profiles across the cross section of the CT are given by Equation 1 and Equation 2 respectively. The bending moment required to bend the CT is given by

$$\text{Equation 4} \quad M_b(R_b) = \left(\frac{E}{2R_b} \right) \left[r_o^4 I_3(\varepsilon_y R_b, r_o) - r_i^4 I_3(\varepsilon_y R_b, r_i) \right] + \frac{4}{3} \sigma_{yp} \left[I_2(\varepsilon_y R_b, r_o) - I_2(\varepsilon_y R_b, r_i) \right]$$

where

$$\text{Equation 5} \quad I_2(t, a) = a^3 \left[1 - \left(\frac{t}{a} \right)^2 \right]^{3/2},$$

and

¹ Relaxing this assumption does not change the argument. The extension to cases where plasticity has not penetrated the inner radius is trivial. However, in problems that involve CT, assumption (v) holds true.

² When CT is bent, the neutral plane shifts towards the side of compression. This shift can be calculated by considering force balance across the CT cross section. For severe bending radii [13], ($R_b < \frac{r_o}{4\varepsilon_y}$) the shift β (with respect to the CT plane of symmetry) is given by one of the roots of the

following quadratic equation:

$$\beta^2 + \left(\frac{1 - 2\mu\varepsilon_{perm}}{\mu} R_b \right) \beta + \left[\frac{2}{3} (r_o^2 + r_o r_i + r_i^2) - \varepsilon_y^2 R_b^2 \right] = 0,$$

where μ is Poisson's ratio. The shift is a very weak function of the permanent strain ε_{perm} and only depends on the bending radius and CT geometry. In general this shift is small enough to be neglected.

Equation 6

$$I_3(t, a) = \sin^{-1}\left(\frac{t}{a}\right) - 0.25 \sin\left\{4 \sin^{-1}\left(\frac{t}{a}\right)\right\}.$$

Equation 4, Equation 5, and Equation 6 agree with the result derived by Yang [19] in Equation 13.

Release After Initial Bend

Releasing the CT is equivalent to applying a bending moment of $-M_b(R_b)$. Therefore the residual stress profile can be calculated by superposing the stresses in the CT caused by the moments $M_b(R_b)$ and $-M_b(R_b)$. Since unloading is elastic (see Timoshenko, 1975, part I, p 95 and part II, p 377), the stress profile due to $-M_b(R_b)$ is given by

Equation 7

$$\sigma_{rel, b}(y) = -\left[\frac{M_b(R_b)}{I_z}\right]y$$

where I_z is the moment of inertia of the CT. The residual stress profile is

Equation 8

$$\sigma_{r, b}(y) = \sigma_b(y) + \sigma_{rel, b}(y).$$

The residual radius of curvature can be found by evaluating the strain in the outermost fibers that did not yield. These fibers are at distances of $\pm \varepsilon_y R_b$ (from the neutral axis), and the strain in them is always proportional to the curvature. Therefore, the residual radius of curvature is

Equation 9

$$\begin{aligned} R_{r, b} &= \frac{\pm \varepsilon_y R_b}{\sigma_{r, b}(\pm \varepsilon_y R_b)/E}, \\ &= \left[1/R_b - M_b(R_b)/(EI_z)\right]^{-1}. \end{aligned}$$

Equation 9 matches with Equation 13 derived by Bhalla [19].

Release after straightening

The stress profile in the straightened CT is described in Table 2. The corresponding straightening moment is

$$\text{Equation 10 } M_s(R_b) = M_b(R_b) - \left(\frac{E}{2R_b}\right) \left[r_o^4 I_3(2\varepsilon_y R_b, r_o) + r_i^4 I_3(2\varepsilon_y R_b, r_i) \right] - \frac{8}{3\sigma_{yp}} \left[I_2(2\varepsilon_y R_b, r_o) - I_2(2\varepsilon_y R_b, r_i) \right]$$

where the functions I_2 and I_3 are defined in Equation 5 and Equation 6 respectively and $M_b(R_b)$ is defined in Equation 4. Releasing the CT from the straight position is equivalent to applying a moment equal to $-M_s(R_b)$. Since the path of unloading is elastic, the residual stress profile at equilibrium is the sum of the stress profile at the end of straightening and the stress profile $\sigma_{rel, s}(y)$ due to the moment $-M_s(R_b)$. This gives,

Equation 11

$$\sigma_{r,s}(y) = \sigma_s(y) - [M_s(R_b)/I_z]y.$$

The residual curvature can be found (as before) from the strain in the outermost fibers that did not yield during loading or unloading. This radius of curvature can be shown to be

Equation 12

$$R_{r,s} = -EI_z/M_s(R_b).$$

Equation 12 is consistent with Equation 13 of Bhalla (1994).

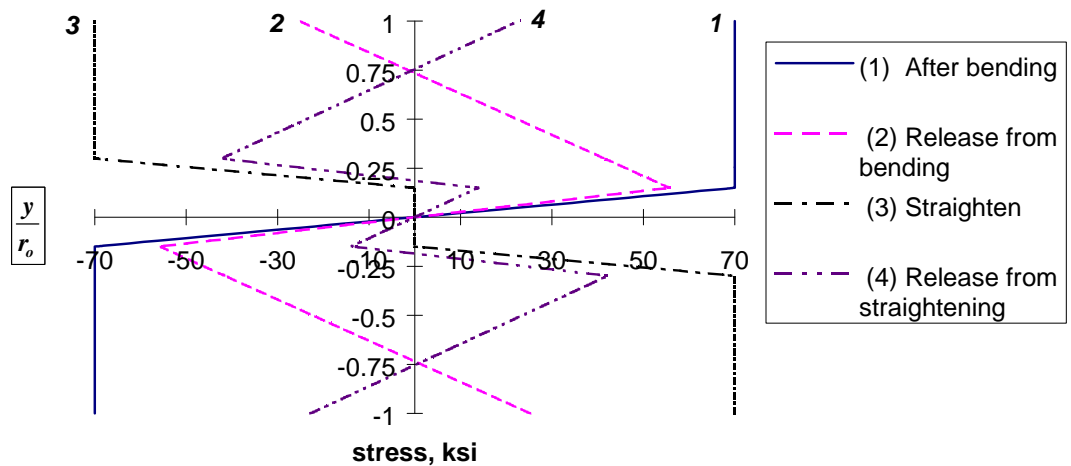


Figure 6 Residual stresses in CT

For 1.5" x 0.109" CT of 70 kpsi material that has been bent to a radius of 48", straightened and released, the residual radius has a value of 20.2 ft.

Figure 6 shows the stress profiles in this CT when it is (1) bent to 48" radius and held there, (2) released, (3) straightened, (4) then released. The peak residual stresses for cases (ii) and (iv) are significant, in this case as much as 58% of the nominal yield stress. These residual stresses will influence the behavior of the CT for all subsequent loading.

COLD WORKING, BAUSCHINGER EFFECT AND CYCLIC LOADING

The stress strain curve obtained from initial loading of a test specimen into plastic range is known as the *virgin curve*. If we apply a load greater than the yield load then remove the load it retains a permanent strain. If we apply another load to the specimen, the reloading portion of the stress strain diagram is, like the unloading portion, approximately a straight line with slope equal to the Young's modulus. The reloading then follows the virgin curve. Similar results are obtained with further loading and unloading. The maximum stress attained before unloading is thus a new yield stress and the material is said to have been strengthened or *work hardened* by plastic deformation (or *cold working*).

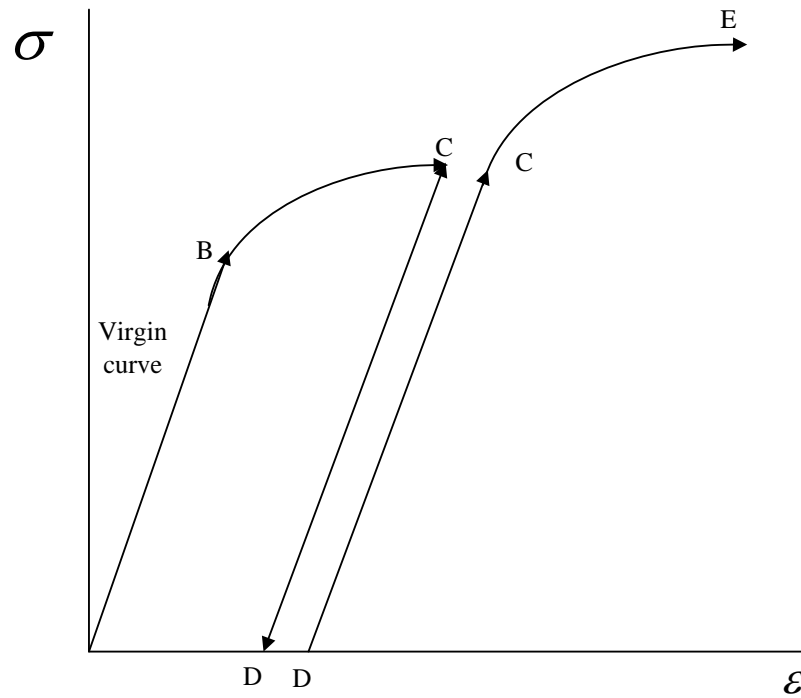


Figure 7 Cold working of ductile materials

If we apply a load greater than the yield load to a metallic specimen, remove the load, then apply the same load in the opposite direction, the material yield point in the opposite direction is reduced. This phenomenon is known as the *Bauschinger* effect. The Bauschinger effect can be observed whenever the direction of straining is reversed. This effect may be explained as the sliding of individual crystals comprising the material and the residual stresses produced by this sliding. Timoshenko [10], Part II, pp. 413-414] provides an appealing phenomenological explanation of this effect by considering the load-elongation characteristics of a set of hinged bars subjected to axial loading. Other explanations based on continuum, microstructural and endochronic approaches have been proposed by various workers. A discussion of these theories is beyond the scope of the present document and the reader is referred to the works by Lubliner [3], pp. 111-113], Yeh et al. [20], Bate and Wilson [21], Schmidt and Morgan [22] and Parker and Kettlewell [23].

From the discussion in the section “Review of relevant literature”, it is clear that coiled tubing is subject to work hardening as well as the Bauschinger effect. For example, the fibers farthest from the neutral axis experience bending strains that are six to seven times the yield strain (as calculated from the uniaxial pull test data). When the tubing is straightened these fibers do not follow elastic-plastic unloading paths. The fibers that experienced tension during bending experience compression when the pipe is straightened and vice versa. When these fibers are subjected to axial loads, they experience tension. This cycle is repeated many times during the life of the CT. Because of the cyclic loading conditions that prevail in CT, the loading/unloading paths can no longer be inferred from the uniaxial material property test data. Experimental data must be obtained by simulating the conditions that CT is subjected to in the field.

DEVELOPMENT OF THE CYCLIC STRAIN TEST (CST)

The aims of the Cyclic Strain Test (CST) are:

- a) to simulate cyclic loading that CT is subjected to when deployed in the field,
- b) to determine the effect of this loading on the material properties of CT.

A CST consists of the following steps:

1. Use the pressurization apparatus shown in Figure 9 to apply the required internal hydraulic pressure.
2. Select the strain range and determine the strain limits for cycling.
3. Load the specimen to the strain determined in step (ii);
4. Unload the specimen and apply load in the opposite direction to the predetermined strain,
5. Repeat (iv) for the required number of cycles.

During the CST, the Data Acquisition System continuously records load, strain (or elongation if using an extensometer), internal pressure and cycle number.

As discussed in the section “Loading events of coiled tubing” of this report, different parts of the CT cross section experience different levels of stress and strain during bending. Typically, the fibers in $\{T_1\}$ and $\{C_1\}$ experience only elastic strains. The fibers in $\{T_2\}$ and $\{C_2\}$ undergo plastic strains that are less than twice the yield strain. The fibers in $\{T_3\}$ and $\{C_3\}$ are subject to plastic strains greater than twice the yield strain. Therefore the matrix of CSTs for this study was designed to reveal the effects of different strain ranges and internal pressure on material properties of coiled tubing. Table 3 shows the test matrix. The maximum strain in tension or compression was 16,000 microstrain. Based on the cyclic strain range, the tests may be classified into the following groups:

- *Full range tests*: The CT is cyclically loaded between ε_{\max} and that $|\varepsilon_{\max}| > |\varepsilon_y|$. For this project, ε_{\max} was approximately seven (7) times the yield strain of 70 kpsi carbon steel for 1.5” OD pipe and five (5) times the yield strain for 2” OD pipe. These are the strain values experienced by the outermost fibers when these pipes are bent over a radius of 48” (the reel radius).
- *Half range test in tension*: The CT is cyclically loaded between 0 and ε_{\max} . This test reflects the actual loading cycle on the outermost fibers in the tension side of the CT when it is bent. More accurately, this is representative of fibers which experience axial strains greater than twice the yield strain (see Figure 4 and discussion in the section “Loading events of coiled tubing”).
- *Half range test in compression*: The CT is cyclically loaded between 0 and $-\varepsilon_{\max}$. This test reflects the loading cycles of fibers on the compression side of the bent CT. This strain range, only represents fibers that experience compressive strains greater than two times the yield strain when the CT is bent.

Table 3 CST matrix for 70 Kpsi samples

CS T	Date	OD (inches)	WT (inches)	Int. press. (psi)	Strain range ($\mu\epsilon$)
1	Jan. 2, 1996	1.5	0.109	0	16,000 to - 16,000
2	Jan. 5, 1996	1.5	0.109	0	16,000 to 0
3	Jan. 5, 1996	1.5	0.109	0	0 to -16,000
4	Jun. 11, 1996	1.5	0.109	2000	16,000 to - 16,000 ³
5	Jun. 11, 1996	1.5	0.109	2000	16,000 to - 16,000
6	Jun. 12, 1996	1.5	0.109	2000	16,000 to 0
7	Jun. 12, 1996	2.0	0.134	0	5,000 to -5,000
8	Jun. 12, 1996	2.0	0.134	2000	5,000 to 0

³ This test was used to debug the data acquisition system and procedure. No useful data was obtained from this test.

TEST APPARATUS, TRANSDUCERS & DATA ACQUISITION SYSTEM

The CSTs were conducted at the Department of Civil Engineering at Rice University, Houston, Texas, following the ASTM E606 guidelines. A tension-compression machine (INSTRON model 1332 with series 8500 controller) was used to perform the tests described in Table 3. The machine is capable of applying 55,000 lbs in tension and compression, and can be cycled between pre-set strain (or stress) limits. The frequency of cycling and the load versus time waveforms are controllable parameters. Axial load is measured by a 250 kN (55,000 lbs) INSTRON tension-compression load cell. The axial strain is measured by an INSTRON 1" gage extensometer. The load cell and/or extensometer outputs are used to control the loading cycles. In addition, a data acquisition system records the axial load and strain continuously in a spreadsheet file. However, this data acquisition system cannot read the internal hydraulic pressure and hoop strain. Therefore, a data acquisition system compatible with the INSTRON machine and controller was built to measure the quantities of interest.

Test specimens

The 3" test specimens were cut from 70 kpsi CT that was never bent. Figure 8 shows a typical specimen. In order to mount the test specimen in the INSTRON machine, a threaded end adapter was welded to each end.

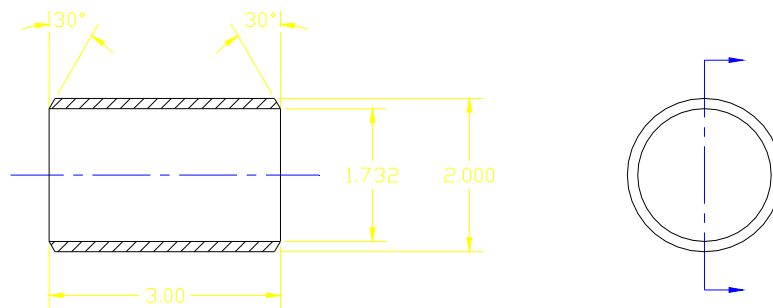


Figure 8 2.0" x 0.134" CT test specimen

Figure 9 shows the complete test fixture with the end adapters. The upper and lower end adapters were machined from 70 ksi 8620 steel and welded on either end of the CT specimen. The ports in the adapters allow the sample to be pressurized. Appendix B contains the drawings of the various parts that comprise the complete test fixture shown in Figure 2.

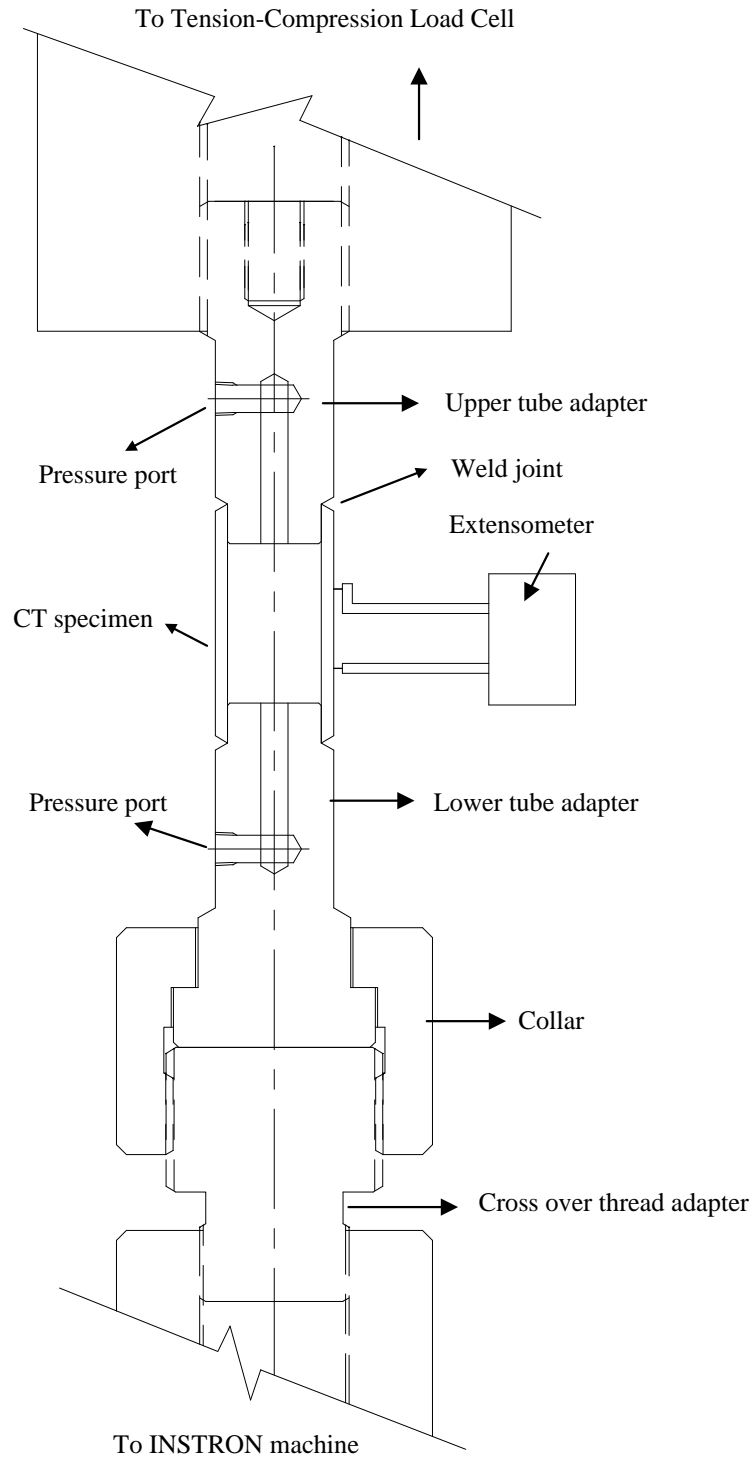


Figure 9 The test specimen with end adapters

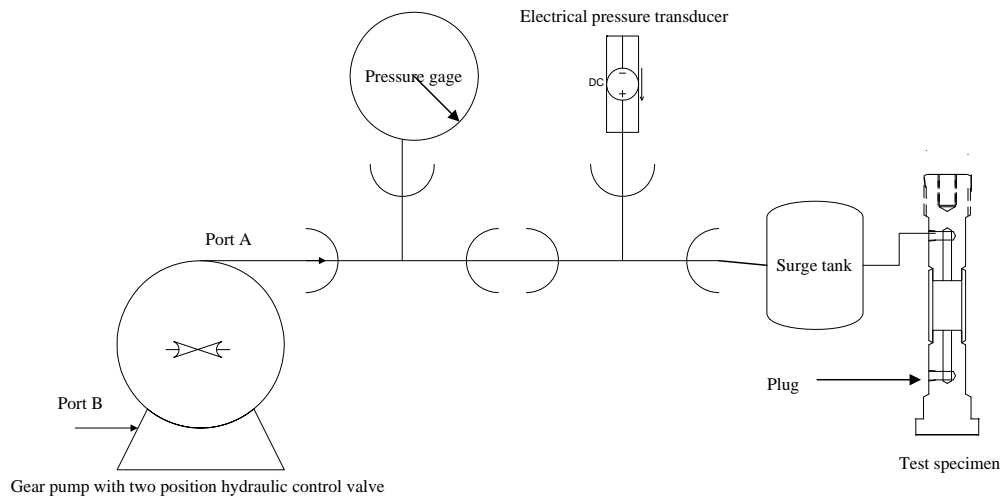


Figure 10 Test specimen pressurization system

Figure 10 shows the schematic diagram of the *test specimen hydraulic pressurization system*. A pump with a two-position hydraulic control valve pumped fluid into the test specimen. Port B was the pressure bypass. Port A was connected to a dial pressure gage, an electronic pressure transducer and a surge tank. The pressure port on the lower adapter of the test specimen was plugged for these tests. The pump was energized after setting the two-position valve to port A. Hydraulic oil was used to pressurize the sample. The sample pressure was relieved by switching the two-position valve from port A to port B. During a CST, the large axial strains change the sample volume. This change in volume would significantly affect the internal pressure for a fixed volume of hydraulic fluid. The pressure in a 3" long test specimen of 1.5" x 0.109" CT subjected to axial strain of 16,333 microstrain increases by 43%⁴. Therefore, a surge tank was designed to ensure that the pressure inside the test specimen did not vary by more than 1%. Appendix C shows the calculations involved in the design of the surge tank.

Transducers

In these experiments, the four primary quantities of interest are axial load, internal hydraulic pressure, axial strain and hoop strain. These are measured by a load cell, a pressure cell, an axial extensometer, and a hoop strain gage respectively. The rate of loading (or the frequency of cycling), and the loading waveforms were also recorded during a typical experiment.

A 250 kN (55,000 lbs) INSTRON tension compression load cell measured axial load. The INSTRON 5000 series controller read the output of the load cell. The controller reads the output of the load cell and converts it to an analog voltage proportional to the load. At full scale, (i.e., $\pm 55,000$ lbs), the output voltage is $\pm 10V$. This voltage is also available to data acquisition systems.

⁴ Assuming that the internal fluid is water or hydraulic oil.

A 0-5000 psi ASHCROFT pressure cell measured internal hydraulic pressure. The pressure cell produces a current signal in the range of 4 to 20 mA. This current through a 250 Ω resistor created a 1 - 5 V signal measured by the data acquisition system.

Axial strain was measured by an INSTRON axial extensometer. The extensometer has a gage length of 1" and is capable of measuring a displacement of 0.5" (or a microstrain of 500,000). The INSTRON 5000 series controller converts the extensometer output into an analog voltage proportional to the strain. At full scale, a voltage of $\pm 10V$ is available at a standard BNC connector on the back panel of the controller. This voltage was fed to our DAQ board.

The hoop strain was measured by a circumferential strain gage. The strain in the gage was measured by a P-3500 strain indicator from Measurement Group, Inc. The strain indicator produces an analog voltage proportional to the strain in the gage.

Data Acquisition System

The Data Acquisition System at Rice University was used for all CSTs, but it can only record the axial load and axial strain. CTES built and programmed a separate Data Acquisition System (DAS) to record the data for tests 4 - 8. This system can continuously record axial load, axial strain, hoop strain and internal pressure. The DAS uses a Data Acquisition board (AT-MIO-64F-5) from by National Instruments, Inc. installed in a Pentium 100 MHz PC. The board has 64 channels of input / output with a 12-bit A/D converter. It can read 64 single-ended or 32 - differential signals. These signals may be bipolar ($\pm 5 V$) or unipolar (0 to 10 V). For the CSTs, the board was configured to read differential signals.

The measurement range of the DAQ system was 10 V (-5 to 5 V), but the range for the load cell and axial extensometer was 20 V (-10 V to 10 V). Therefore, voltage attenuators such as in Figure 11 were used on the axial extensometer and load cell channels. The circuit reduced the voltage by a factor of 3 before feeding it to the DAS. The voltage that is read by the DAS is given by

$$V_{\text{DAQ}} = \frac{R_G}{R_E + R_F + R_G} V_{\text{transducer}}$$

The number of loading cycles and the strain rates were recorded manually from the control panel of the INSTRON machine.

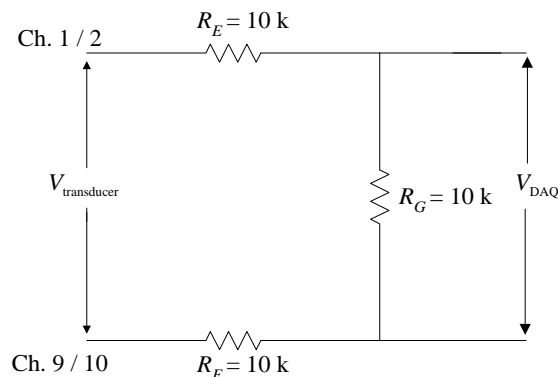


Figure 11 Attenuator circuit for DAQ board

EXPERIMENTAL DATA FROM CST

Figure 12 shows the uniaxial stress-strain curve for a virgin sample of CT when it is pulled for the first time. The figure confirms the linear behavior of CT material in the elastic range. The sample yields abruptly and the strain increases without corresponding increase in stress. This is a good example of elastic-perfectly-plastic behavior. When the specimen is unloaded, the sample retains a permanent strain as shown in Figure 13. The sample must be compressed to return it to its original length (zero strain). When the sample is loaded in compression, the stress-strain curve follows an elastic linear loading path (parallel to path 1-2) until the stress disappears. Further compression results in a highly nonlinear stress-strain curve.

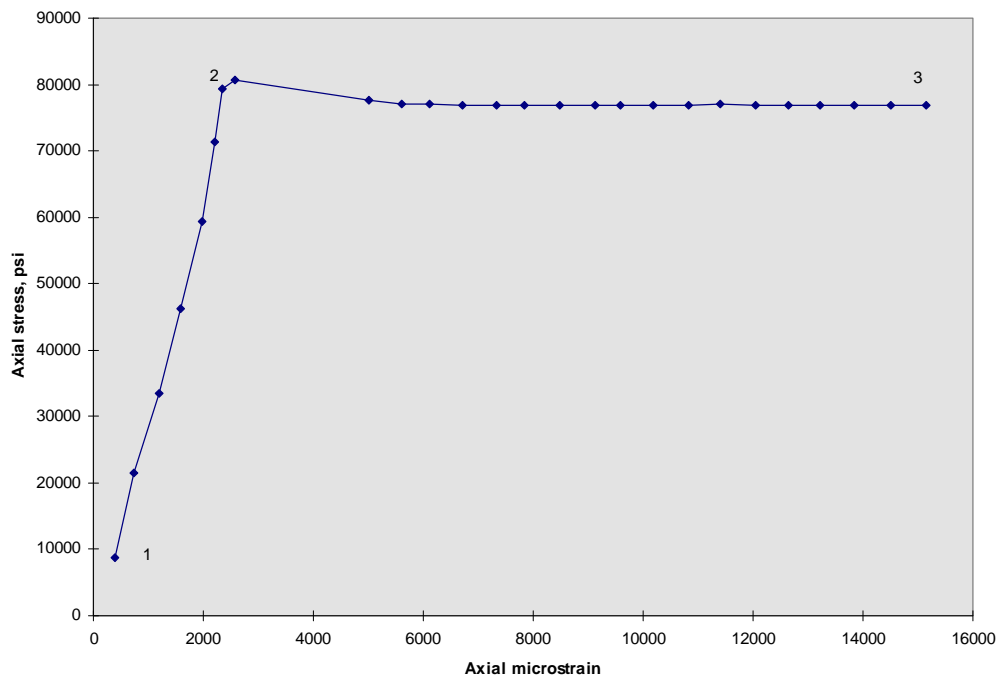


Figure 12 Axial loading of virgin sample, CST # 1

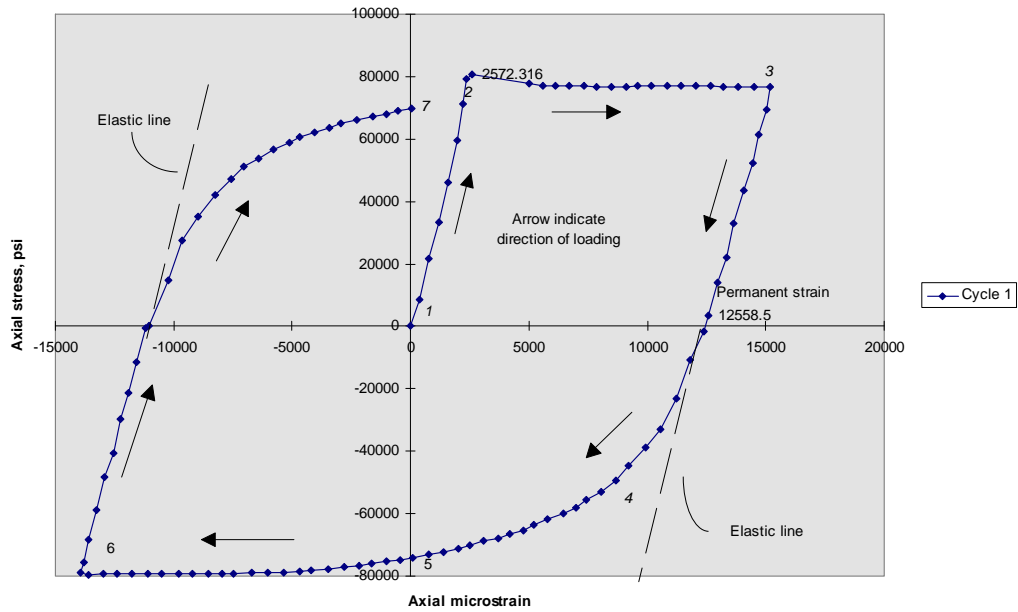


Figure 13 The Bauschinger effect in CT steel, CST # 1

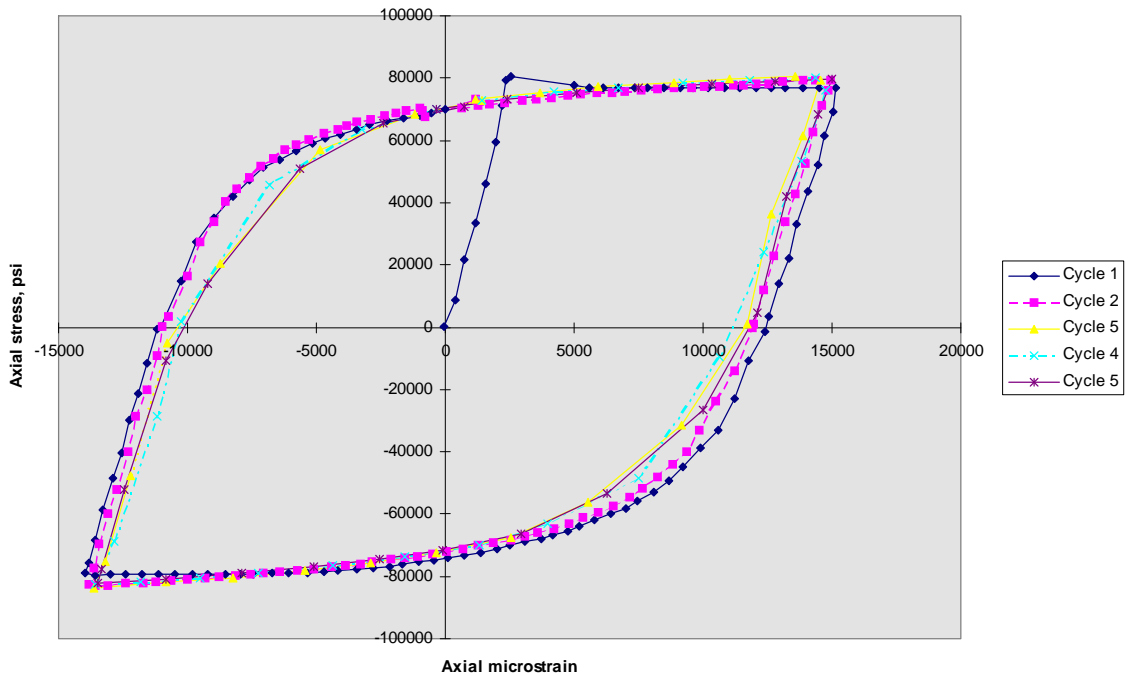


Figure 14 Cyclic loading of CT specimen, CST # 1 – First 5 Cycles

This illustrates the well-known Bauschinger effect. Increase in strain is necessarily accompanied by increase in stress, and we begin to see the effects of *cold-working* or *strain hardening*. The Bauschinger effect occurs again when the direction of loading reverses again (at point 6 in Figure 13). In the absence of the Bauschinger effect, point 7 would be at the same stress as point 2.

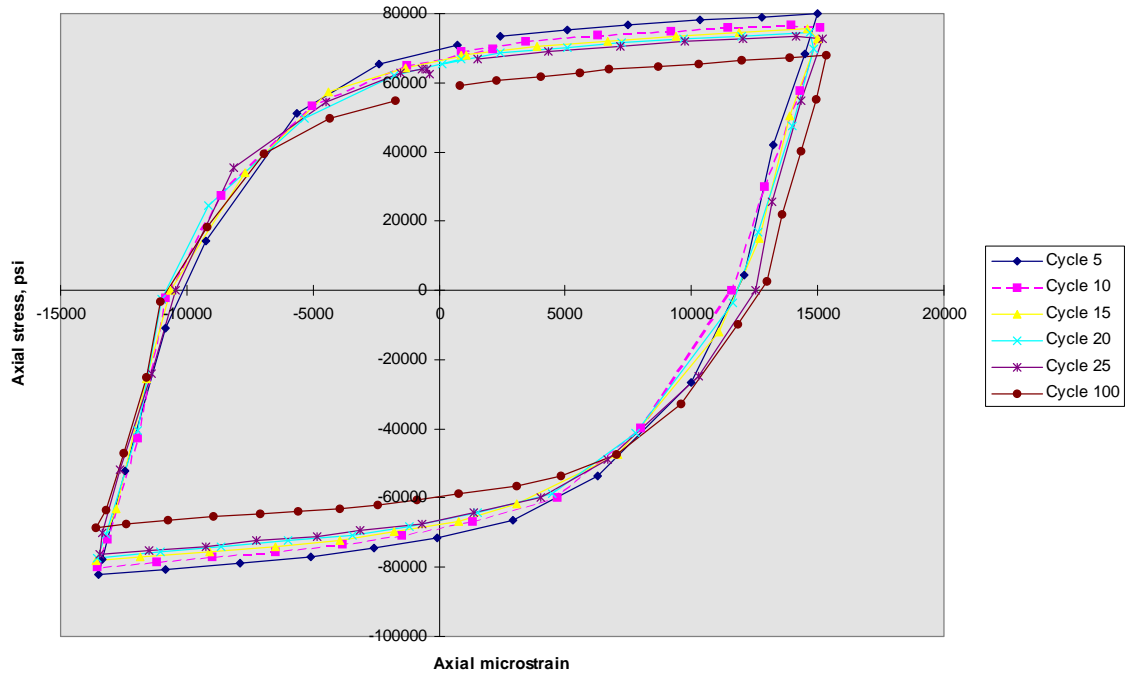


Figure 15 Cyclic loading of CT specimen, CST # 1 – Selected Cycles

The stress at the end of each cycle can therefore be used as a measure of the change of material properties with increasing number of cycles. Figure 14 shows the stress-strain curve for the same specimen for the next five CST cycles. Note the gradual shift of the elastic portion of each curve towards the stress axis. Figure 15 shows the percentage change of stress (with respect to the nominal yield stress of the material) at point 7 as a function of the number of loading cycles.

Figure 16 and Figure 17 show stress-strain data for the half range tension and compression tests respectively. As expected, the material behavior curves are geometrically similar to the curves obtained from the full-range tests. The Bauschinger effect, elastic unloading, and departure from linear behavior (after the first pull/compression) are evident in both tests.

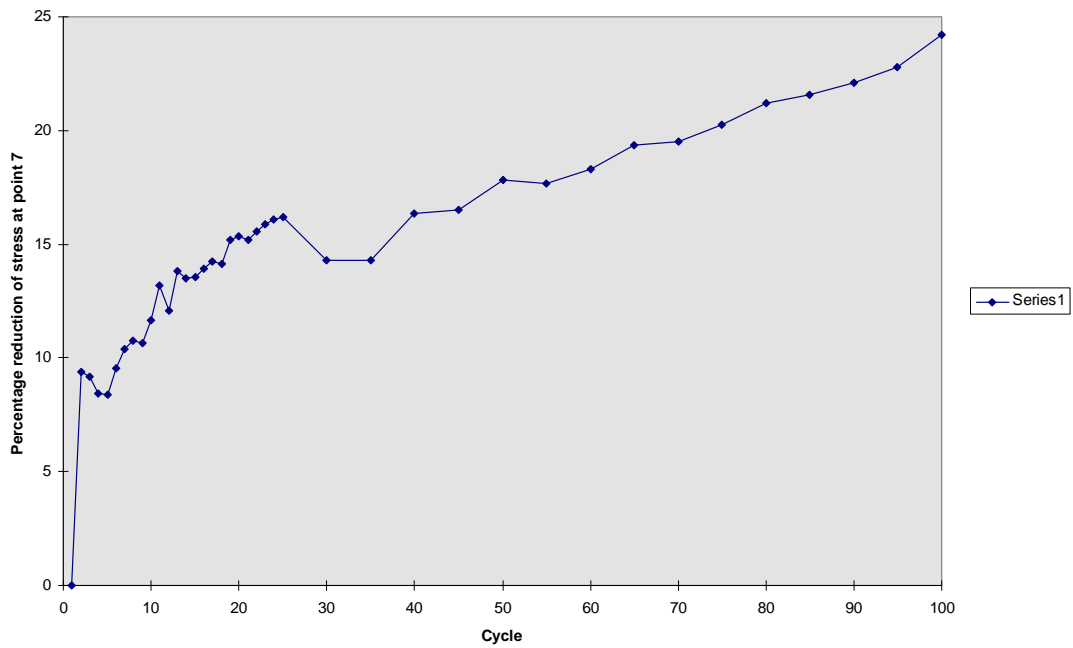


Figure 15 Change of yield stress with cycling, CST #1

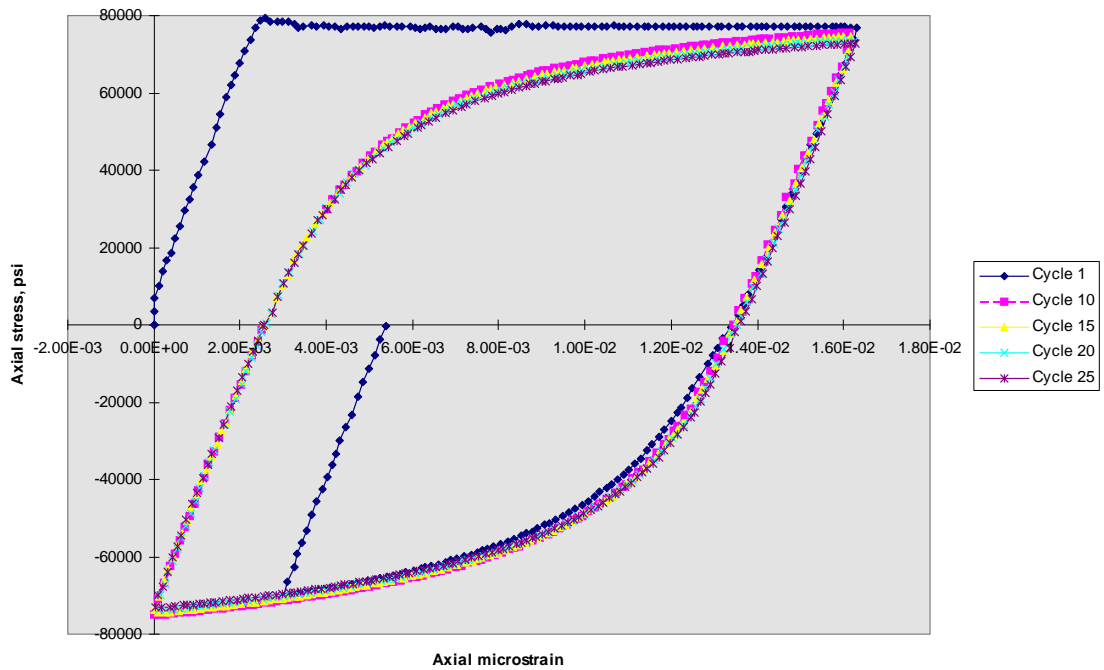


Figure 16 Half range tension test, CST #2

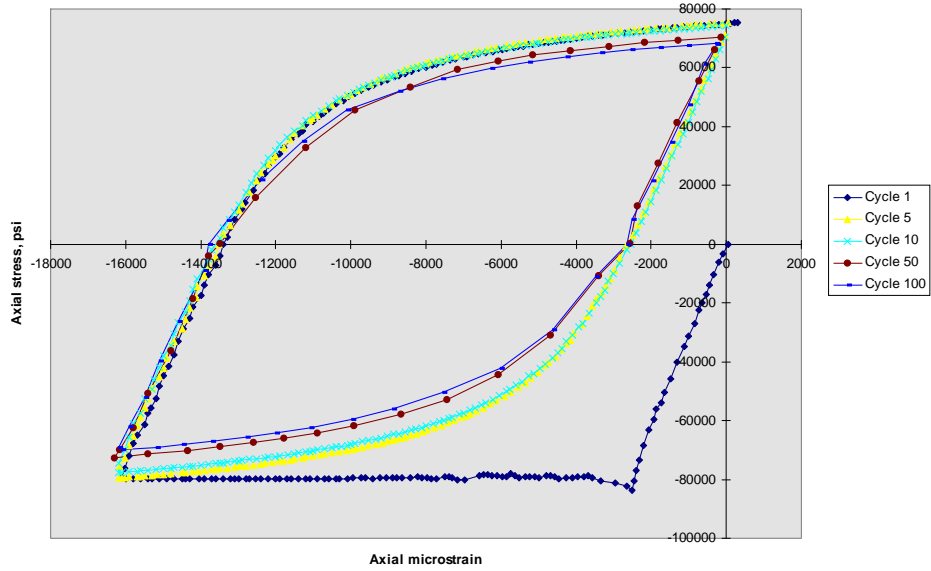


Figure 17 Half range compression test, CTS #3

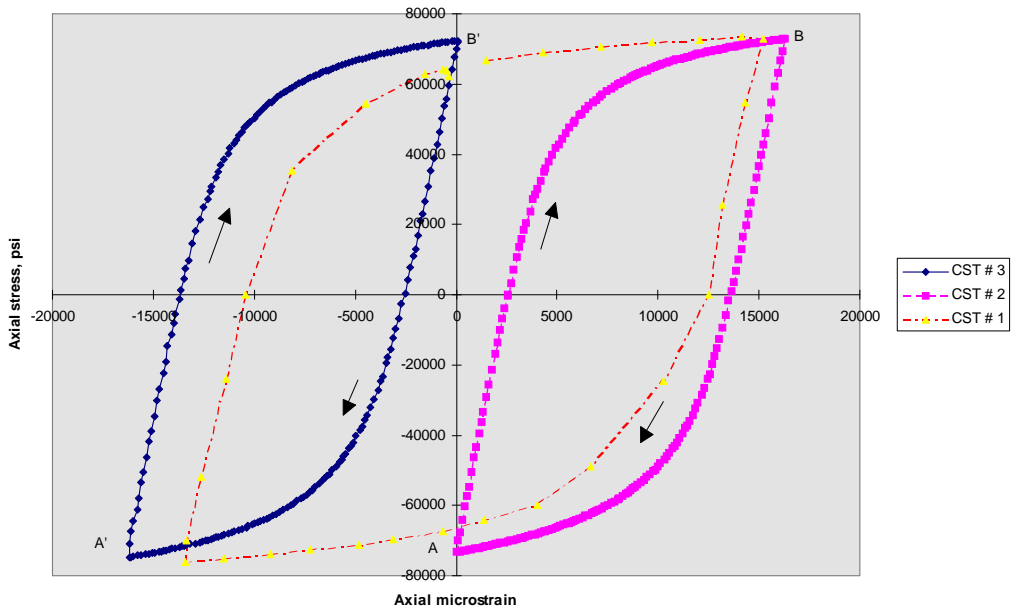


Figure 18 Cycle 25 for CST #1, #2 and #3

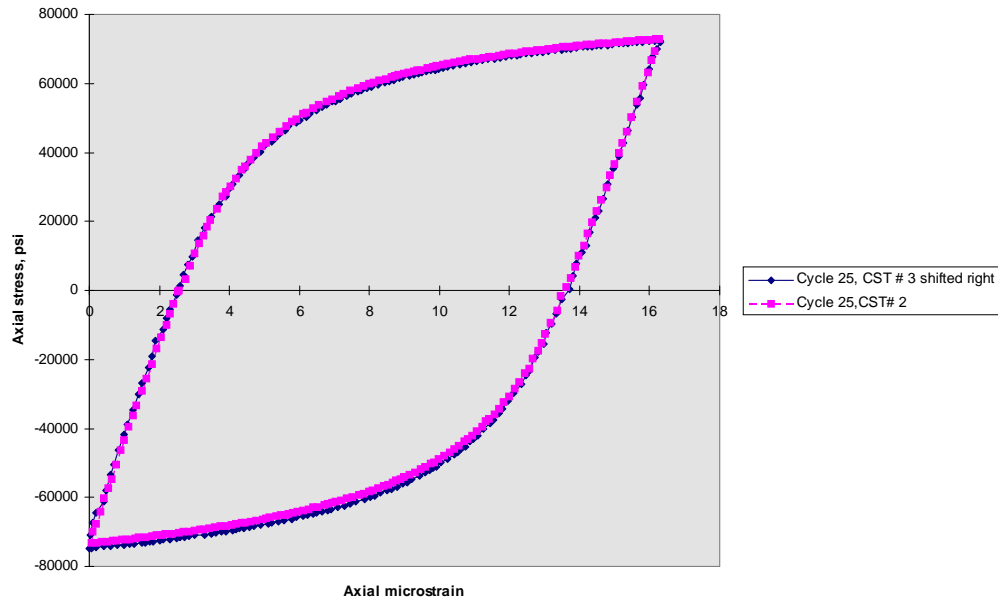


Figure 19 Symmetry of the half range tests, CST # 2 and # 3

The yield strength decreases very rapidly (about 15% in the first twenty cycles) in the first few cycles and then reaches an approximate steady state. In Figure 18, the 25th cycle is plotted for tests 1, 2 and 3. Figure 19 confirms the geometric similarity of the curves shown in Figure 18. In this figure, cycle 25 of CST # 3 is superimposed on cycle 25 of CST # 2. The result suggests that the material property curves from cyclic loading are self-similar. Objects that are geometrically similar on all length scales are said to exhibit self-similarity. All self-similar quantities obey simple power laws and they are used in the study of fractals. (An example is Newton’s law of gravity which varies as the inverse square of length on all scales.) Self-similarity implies that a two dimensional curve, for example the stress-strain curves discussed thus far may be expressed as [24]

$$f(x,y) = x^\alpha g(y/x^\beta)$$

in which $f(x,y)$ has been replaced by a function of only one variable g . For any range of the variables over which g is relatively constant, $f(x,y)$ is then approximated by a simple power law in x . The constants α and β could be determined for different materials and strain ranges. In other words the constant β and the scaling function g are the properties of the material under cyclic loading. These properties (along with the modulus, yield stress, etc.) can be determine once and for all and provided to the field engineer. The cyclic stress-strain curve for the appropriate strain range can then be recovered from the scaling equation. Such stress-strain curves resemble the “hysteresis” curves encountered when a piece of iron is magnetized by a current that changes magnitude and sign in a prescribed cycle [25]. Fractal scaling laws have already been used in the analysis of ferromagnetism where similar “hysteresis” type material behavior is encountered [24].

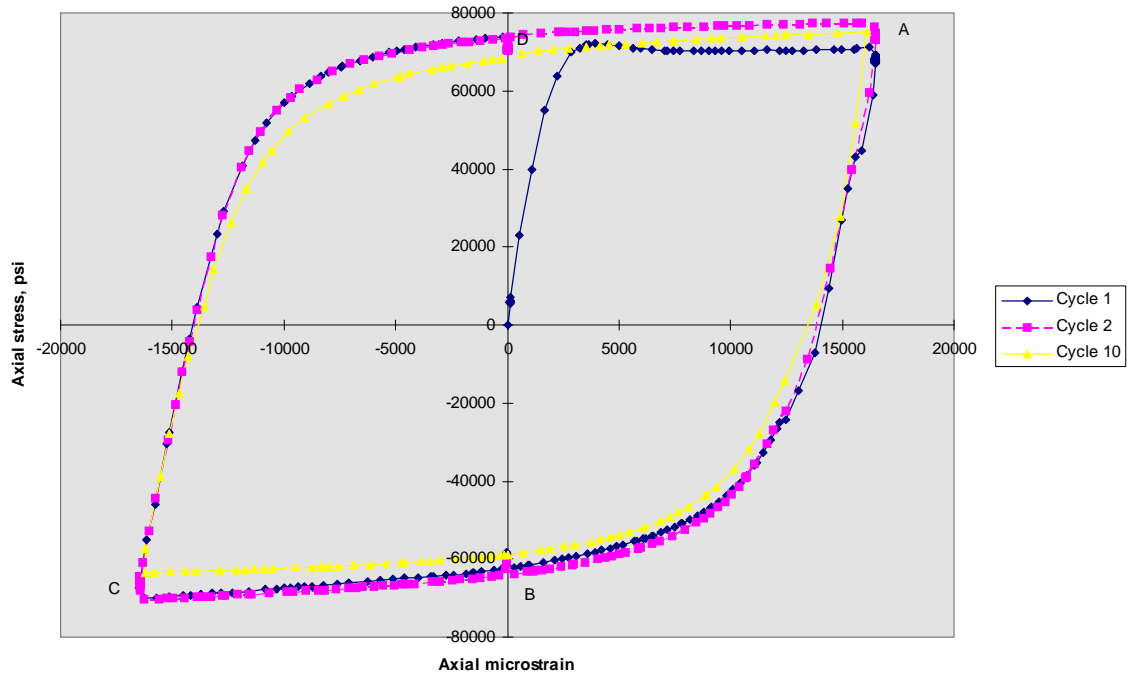


Figure 20 Full range test with 2000 psi internal pressure, CST # 5

Test specimens subjected to cyclic loading with internal hydrostatic pressure, experience triaxial stress as described in the section “Loading events of coiled tubing”. In the elastic range, the radial, circumferential and axial stresses are given by Equation B 2, Equation B 3 and Equation B 4 of Appendix B. The first term in Equation B 3 represents the contribution of internal pressure p_i (pressure cell reading) to the axial stress and the second term is the contribution due to the directly applied axial load P (the load cell reading). At any point in the loading cycle, the axial stress must be computed from the load cell and pressure cell readings by using Equation B 4. Figure 20 shows the cyclic axial stress/axial strain profile for a test specimen with internal pressure. This figure resembles the curves shown in Figure 14 and Figure . In fact, the material yield strength remains unchanged (as expected). The yield load is however reduced in tension because of the effect of internal pressure. Consider Figure 21 which shows the variation of the axial stress with the circumferential (hoop) strain for the same test. At zero axial load (the load cell reads zero), the hoop strain from Equation B 6 is approximately 300 microstrain.

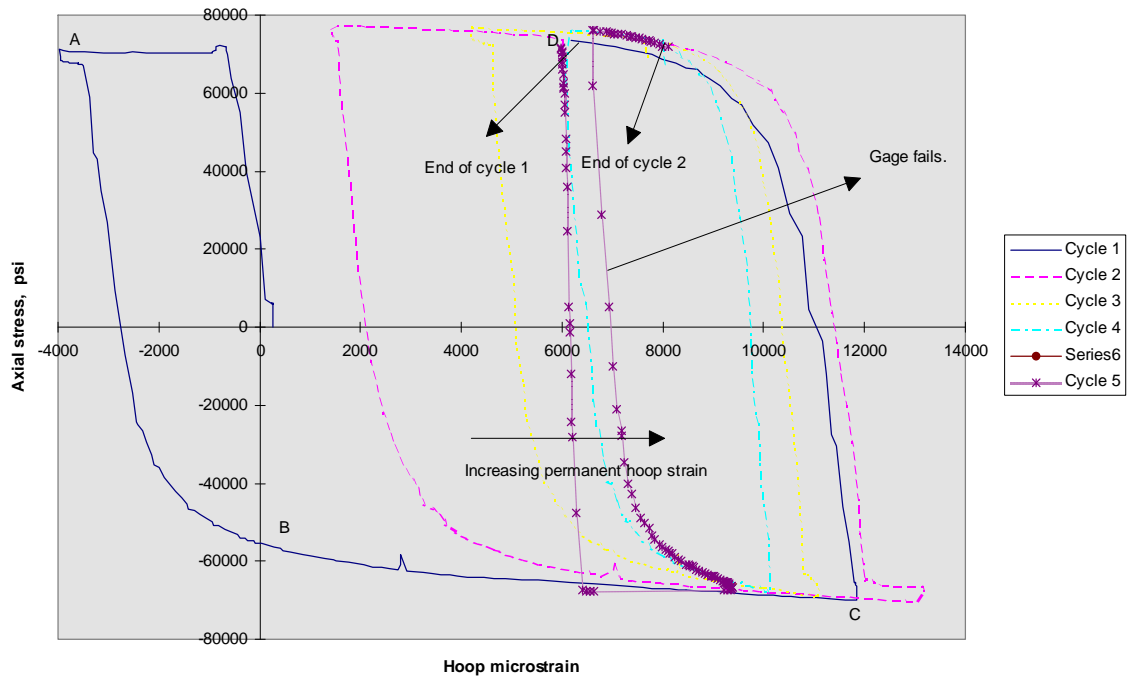


Figure 21 Hoop strain in full range test with 2000 psi internal pressure, CST # 5

As the sample is loaded in tension, the hoop strain decreases and eventually becomes negative. When the axial stress is large enough, the second term in Equation B6 dominates and the hoop strain is negative. When the sample yields, the hoop strain decreases without further increase in axial stress. The circumferential and radial stresses do not change (see Equations B2 and B3) since the pressure is constant. The variation in the hoop strain is only due to the change in axial stress (and hence axial strain). Note that at the end of the cycle (point D in Figure 20 and Figure 21) the axial strain is zero but the hoop strain is approximately 6000 microstrain. The permanent hoop strain at the end of cycle # 1 is the *diametral growth*. The diameter increases with each cycle. This result clearly proves that plastic cycling under internal pressure causes ballooning of CT.

Figure 22 and Figure 23 show data from a half range tension test. The behavior is similar to the that of the full range tests.

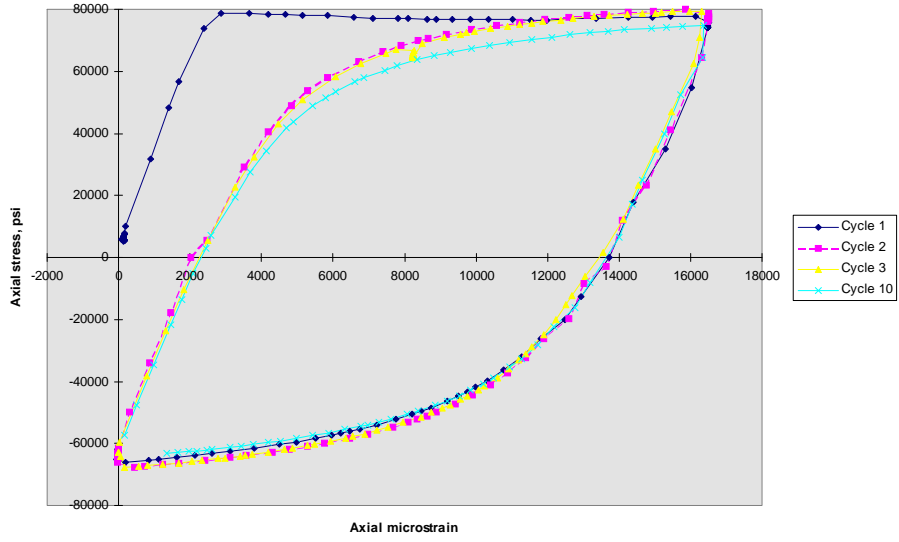


Figure 22 Half range tension test with 2000 psi internal pressure, CST # 6

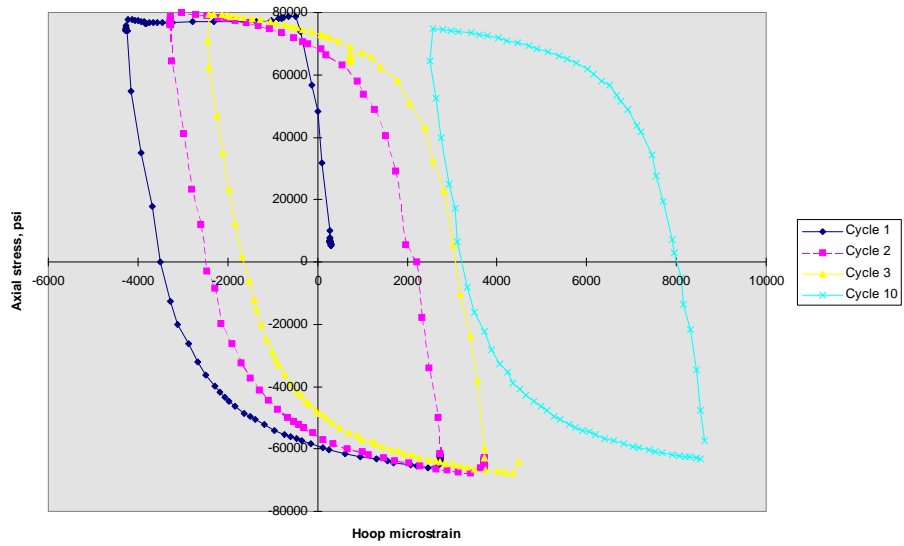


Figure 23 Hoop strain half-range tension test with 2000 psi internal pressure, CST #6

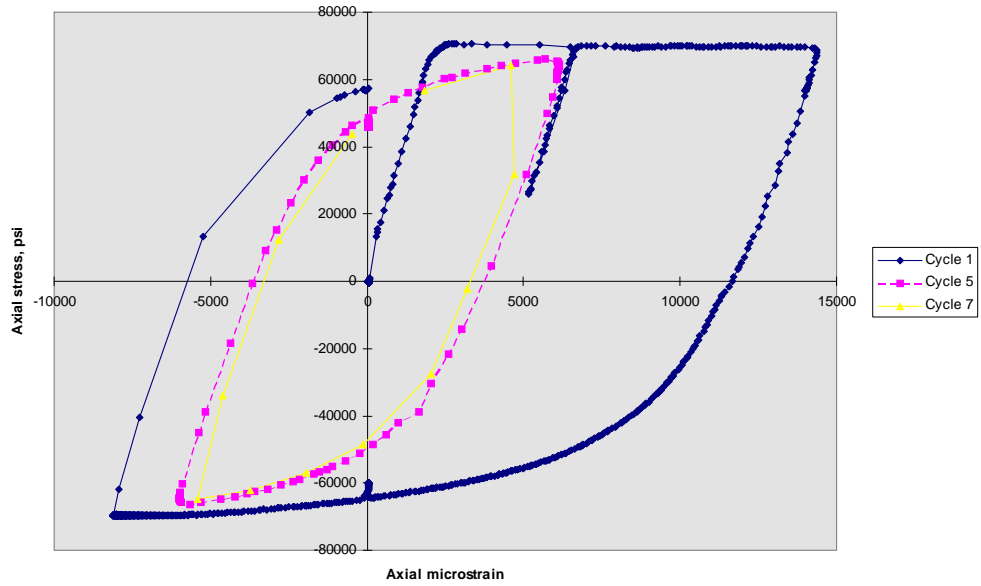


Figure 24 Full range test for 2'' OD CT- axial strain, CST # 7

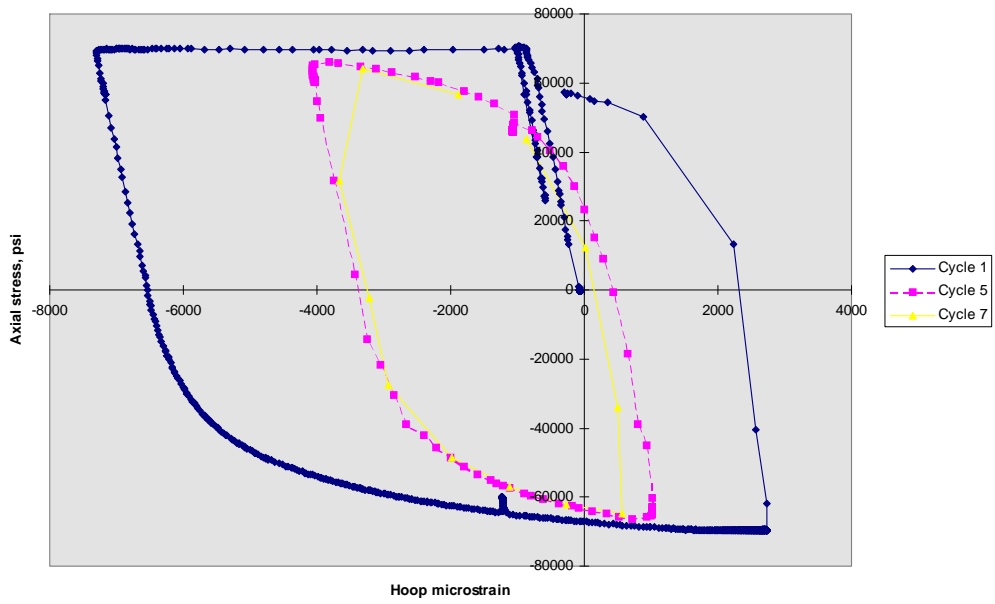


Figure 25 Full range test for 2'' OD CT- hoop strain, CST # 7

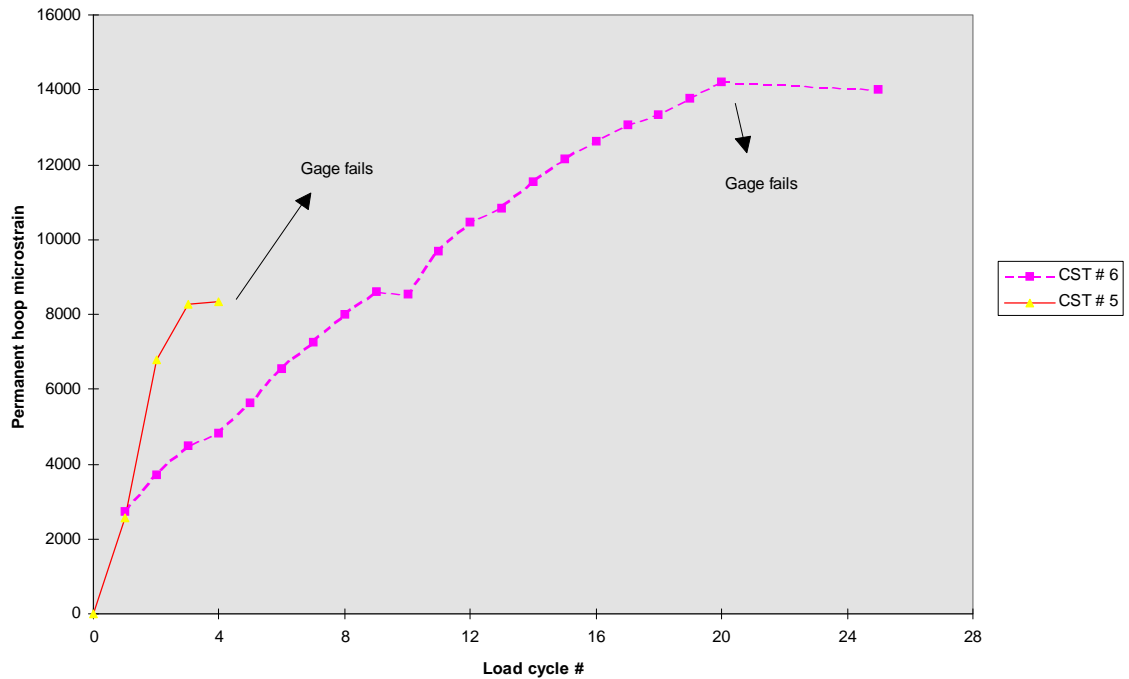


Figure 26 Diametral growth for CST # 5 and # 6

Note the geometric similarity between the half and full range tests. Figure 24 and Figure 25 illustrate the material behavior for the full range test of 2" x 0.134" CT. Figure 25 proves that internal pressure is necessary for ballooning. Figure 26 shows the diametral growth as a function of the number of load cycles. The hoop strains plotted along the y-axis axis are measured when the axial strain is zero and the axial stress is compressive. There appears to be a qualitative difference in the behavior of the diametral growth in the two tests. Recall that CST # 5 was a full range test while CST # 6 was a half-range tension test. In other words the strain range in CST # 6 is half the strain range in CST # 5. Correspondingly, the diametral growth for a given number of cycles for CST # 6 is a little greater than half the diametral growth for CST # 5. This is a very qualitative observation and more data is required to quantify this effect. For CT in the field, the ballooning will be less severe than that observed in Figure 26 because the strain comes from bending. The fibers close to the neutral axis of bending do not suffer any plastic deformation while those far removed from it experience severe plastic strains.

Incipient yield criteria

A yield criterion describes the conditions under which yielding occurs in a body. Mathematically it is represented by a function $f(\sigma_{i,j}, \sigma_{yp})$ where $\sigma_{i,j}$ defines the (triaxial) state of stress and σ_{yp} is the uniaxial yield strength in tension or compression [2]. When $f(\sigma_{i,j}, \sigma_{yp}) < 0$ the stress state is elastic. According to the incipient yield criterion, yielding begins when $f(\sigma_{i,j}, \sigma_{yp}) = 0$ at any point in the body. For CT subjected to radial, hoop, and axial stresses, the von Mises yield criterion states that

Equation 13
$$f = (\sigma_{rad} - \sigma_h)^2 + (\sigma_h - \sigma_a)^2 + (\sigma_a - \sigma_{rad})^2 - 2\sigma_{yp}^2.$$

The principal difficulty in applying such incipient yield criteria is that the limit state is determined by the first point satisfying the condition $f(\sigma_{i,j}, \sigma_{yp}) = 0$. Secondly, the criterion assumes a sharply defined yield point.

Consider the case of CT that has been bent and straightened at zero internal pressure ($\sigma_{rad} = \sigma_h = 0$). The stress profile across the cross section of the CT is shown in Figure 6. All fibers at distances greater than $2\varepsilon_y R_b$ from either side of the neutral axis are at tensile or compressive yield stress. Hence, according to Equation 13 the CT has already failed. However, the CT can support axial loads. In the absence of internal pressure, the CT can support tensile axial loads up to the yield load of the virgin CT [12], [15]. All fibers in the range $r_o \geq y \geq -2\varepsilon_y R_b$ are capable of elastic deformation and can support axial loads. Thus, the incipient yield criterion failed to predict the limit state of the CT. Despite significant residual stresses in (large) portions of the cross section, the CT retains strength on a "global" basis. Thus "incipient yield" is too stringent a criterion. Clearly, the situation gets more complicated when the CT is subjected to internal pressure as the stress state is triaxial. Therefore, a more accurate limit state is needed.

When a body is subjected to stresses beyond the yield point, the state of stress for additional loading depends on

- i. the initial state of stress,
- ii. the path of loading (and hence the material property curve), and
- iii. the geometry of the body.

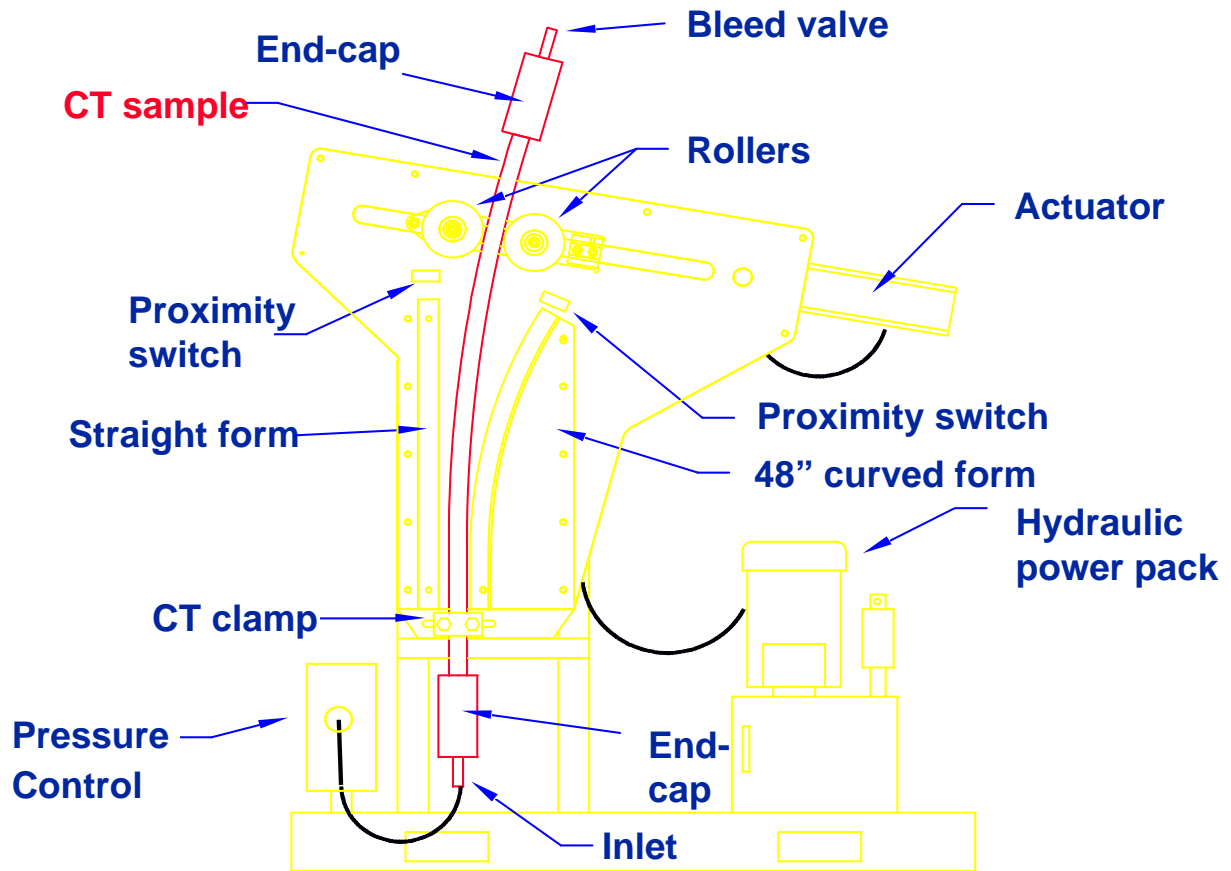


Figure 27 Fatigue Test Machine (FTM)

Furthermore, the order in which the body experiences different loading events becomes important. For example, bending followed by axial loading beyond the elastic limit is not the same as axial loading followed by bending beyond yield. Therefore, the procedure to determine the new CT limits should account for:

- residual stresses prior to a loading event,
- the change in material properties,
- "complete" failure (as opposed to local yielding) of the CT by including geometry dependent parameters.

The procedure requires rigorous analysis of CT mechanics and subsequent experimental verification.

Test apparatus necessary to verify the CT limit states should be able to simulate the states of triaxial stress in CT in the real world. It should be capable of bending CT around different radii of curvature with or without internal pressure and applying axial loads on CT.

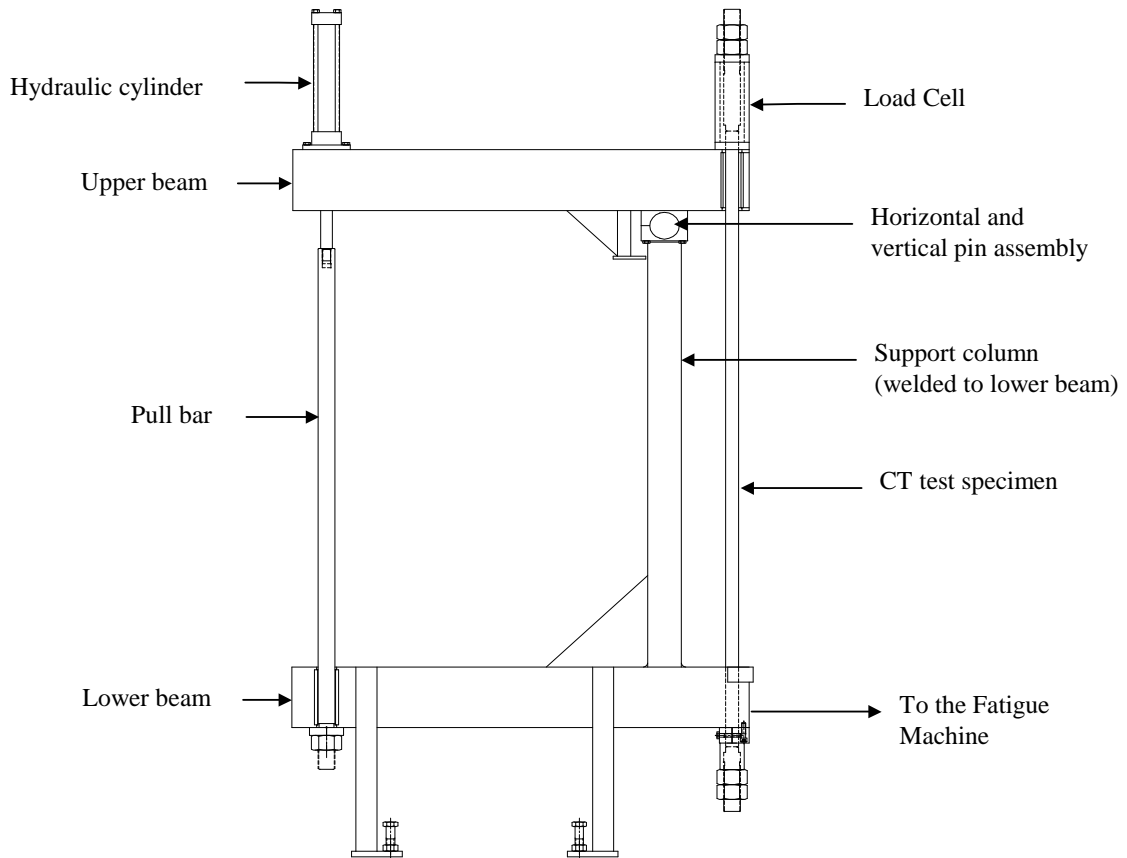


Figure 28 Axial Loading Fixture (ALF)

Figure 27 shows a Fatigue Test Machine (FTM) to simulate CT fatigue. Figure 28 shows an Axial Loading Fixture (ALF) which operates in conjunction with a FTM by exerting an axial load on the CT when it is in a straight position. The lower beam of ALF is attached rigidly to the FTM perpendicular to the plane of bending of the CT. The upper beam pivots on the support column via a pin assembly and can rotate in a plane normal to the plane of the figure. The CT test specimen is attached to the upper and lower beams as shown in Figure 28. The load cell measures the axial force on the test specimen. The hydraulic ram exerts axial force (tension) on the pull bar. Retracting the hydraulic ram pulls on the CT specimen with a force approximately five times greater than the tension in the pull bar. The force is amplified and transmitted as tensile load to the CT. The CT must be in a "straight" position when it is attached to the ALF. A typical test procedure with this fixture consists of the following steps:

1. Attach the lower beam of ALF to the fatigue machine.
2. Load the test specimen into the FTM (and pressurize it if necessary).
3. Bend and straighten the CT for the required number of cycles.
4. With the CT in the straight position, attach the upper beam of the ALF to the CT.
5. Apply tension on the CT by pressurizing the hydraulic cylinder to retract the ram.
6. Remove the axial load and detach the upper beam from the CT.

Repeat steps 3 to 6.

Limit states applied to design

According to traditional design philosophy, Working Stress Design or WSD, the design limits of a system are determined by a 'factor of safety', $SF = R_n / R_w$, where R_n is the nominal resistance and R_w is the safe working magnitude of a given parameter. R_n is determined from theory or experiment while R_w is chosen based on experience and/or observation. In other words, this approach compares an "estimated" most severe loading condition that can occur on a system with its "known" least capacity. The margin of safety is determined by SF .

In contrast, a reliability-based design approach has its basis in probability. According to Payne and Swanson [26] the expected load l on a system and its resistance (or capacity) c are both treated as random variables. These random variables model the variability of design loads, material properties, and geometry of the structure. The variability (or uncertainty) in each factor is indicated by the statistical spread in the data. The goal is to ensure that the capacity always exceeds the load. The design fails when $c < l$. The reliability of the design is quantified by the mathematical probability that c is always greater than l . In essence, the magnitude of $c - l$ defines the "limit state, g " of the system. The design is safe for positive values of g and unsafe for negative values. References [26] - [29] contain further details of this method, which is known as Load and Resistance Factor Design (LRFD).

An LRFD based approach would be a good method for defining CT limit states. The problem of determining the limit states of CT is essentially the inverse of a design problem. In a design problem, a structure is designed to meet certain load requirements or reliability criteria. The limit state is a "known" quantity while the design variables are unknown. For CT, the limit states or probability of failure is the unknown quantity while the design variables and loads (or their probability distributions) are known. The ultimate limit state of CT for a given load is a function of its initial or residual stress profile, its loading path, material properties, and geometry. An LRFD based approach would eliminate the need for exact knowledge of these parameters during the determination of the limit states. Instead, the "risk of failure" for each loading condition could be assessed. This approach would require a statistically large enough data base to estimate the distribution of parameters.

COILED TUBING TEST MACHINE

CTTM Description

A new Coiled Tubing Test Machine (CTTM) was developed to simulate the bending and force environment CT is exposed to. Appendix A gives the specifications for the design of this machine. The CTTM is able to bend the CT sample around a fixed radius of curvature and straighten it again with internal pressure, in a similar manner to other existing fatigue test machines. Different radii of curvature are achieved by changing the bend form. The CTTM has the additional capability of being able to apply constant tension up to 200,000 lbs, (including constant tension while bending) and the capability of rotating the sample while in the straight position, allowing cycles of rotation and then bending. Figure 30 is a picture of the CTTM.



Figure 30 – Coiled Tubing Test Machine

The “bend table” at the center of the machine contains a curved form below the CT sample and a straight form above the sample. The bend table moves upwards to bend the CT around the curved form, then downwards to straighten the CT against the straight form. As stated above, changing out the bend form allows for multiple radii of curvature. The 2 pictures in figure 31 show the bending sequence. The picture on the left shows the bend table in the down or straight position. The right picture shows the bend table in the up or bent position.

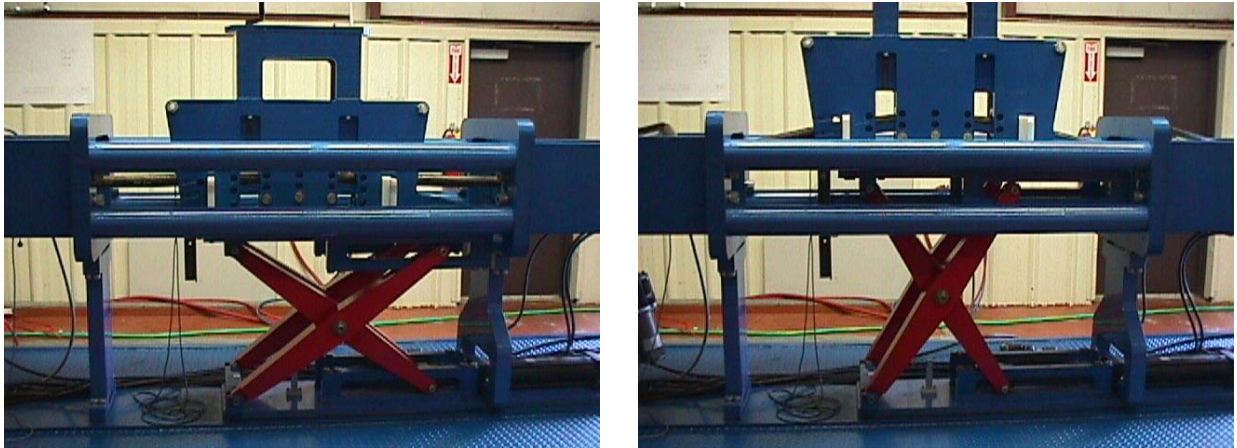


Figure 31 – Bend Table in the Straight and Bent Positions

Large hydraulic cylinders at the ends of the CT sample maintain the desired tension in the CT while bending, or apply the desired tension between bends. A servo-motor rotates the CT between bends. The control panel is shown in Figure 32.

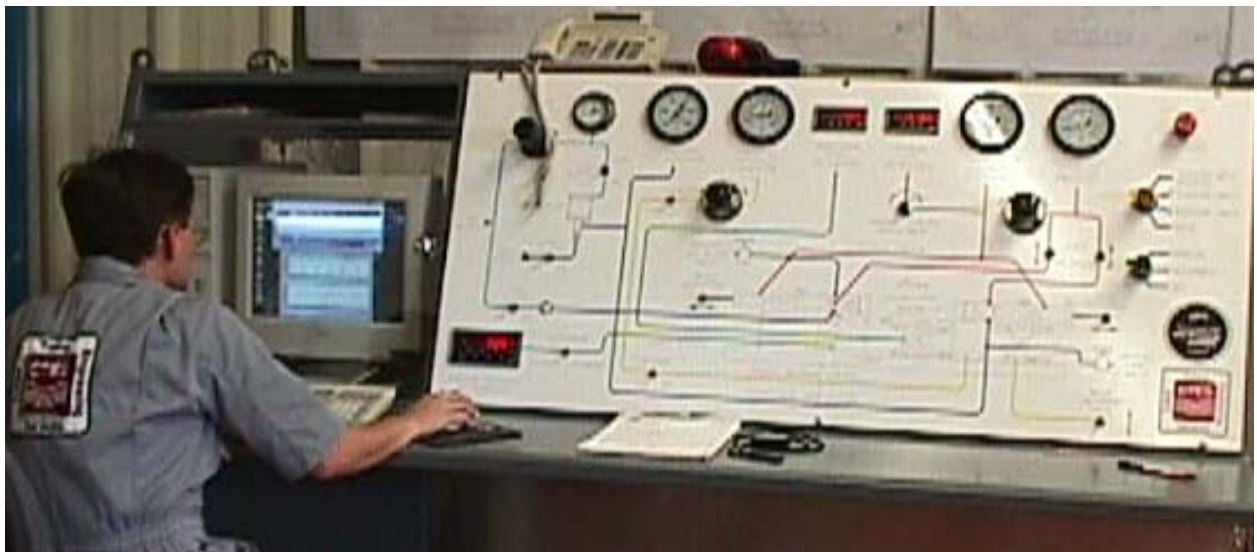


Figure 32 – CTTM Control Panel

The machine can be controlled either automatically from the PC or manually from the control panel. Data such as cycles, tension, internal pressure, and rotation position are recorded automatically. Both the control function and the data acquisition are performed by a CTES Orion CT data acquisition system. The upper window in Figure 33 is the CTTM control program. The lower window is the Orion data acquisition software.

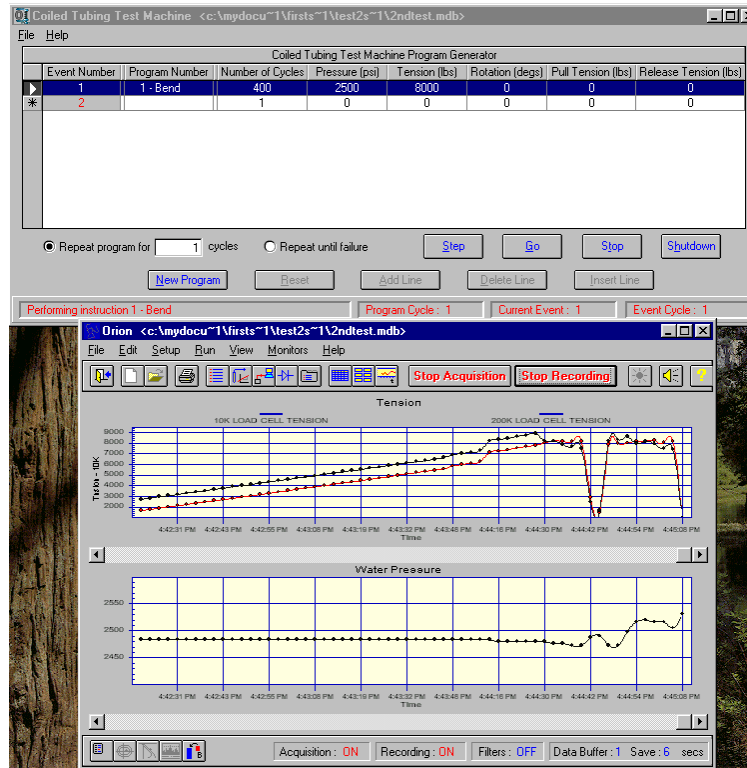


Figure 33 – CTTM Control and Data Acquisition Software

Testing designed to increase the understanding of internal pressure with tension and internal pressure with tension and rotation was conducted to improve the understanding of CT fatigue. Unfortunately, only a limited number of tests were performed before the funding was eliminated.

CTTM Capabilities

- 1) CT OD = 1.25" - 3.50"
- 2) Tension
 - During bending = 10,000 lbs
 - Without bending = 200,000 lbs
- 3) Sample maximum internal pressure = 10,000 psi
- 4) Bending to yield = 3.5" OD x 0.25" wall CT, 100 kpsi material
- 5) Bending radii
 - 1.25" - 1.50" CT = 48"
 - 1.75" - 2.38" CT = 72"
 - 2.88" - 3.50" CT = 100"
- 6) Rotation of CT sample about longitudinal axis (azimuth increment = 10°)

CTTM Features

- 1) Short CT sample length (nominally 109")
- 2) Automatic or manual control
- 3) Skid-mounted
- 4) One-man operation
- 5) No welding on CT sample (hydraulically-operated slips)
- 6) Precision load cells to measure tension
- 7) Extensometers to measure axial strain
- 8) Electronic pressure transducers
- 9) LVDT to measure travel of bending form

Automatic Measurements During Operation

- 1) Tension during bending
- 2) Tension without bending
- 3) CT sample internal pressure
- 4) Axial strain (elongation)
- 5) Hydraulic pressures
- 6) CT sample azimuth angle (orientation)
- 7) Bending form vertical position (LVDT and inductive proximity switch)
- 8) Straight form vertical position (inductive proximity switch)

Mechanics and Hydraulics

Grips

The grip mechanisms for each end of the CT are identical. A single piston applies force to a set of grip blocks that slide along a tapered cam. An internal mandrel machined to fit snugly within the CT is inserted inside the CT. The grip blocks press on the outside of the CT and grip the CT between the blocks and the internal mandrel. Two pressure lines are connected to the piston. via a 4 way, 3 position solenoid activated valve. Two pilot activated check valves are in the circuit to ensure pressure is maintained in the piston chambers. By activating the valve, pressure is either ducted to the gripping or releasing side of the piston, while the alternate side is ducted to tank (see Figure 7100-1004-16). The CT ends are also sealed inside the grips. The seals are capable of holding 10,000 psi of water with a reasonable safety factor.

Bend Table

A hydraulic cylinder powers the bend table. Using an "X" type mechanism, the table is lifted or lowered by alternating the side of the piston to which pressure is provided while venting the other side to tank.

The bend form is made up of a lower curved component with a radius equal to the desired bend radius and an upper strait form used to straiten the pipe. The strait portion of the bend form can be lifted using a hand crank to allow for multiple sized tubing and for ease of insertion of the CT. Once the CT is installed in the machine, the strait form is lowered to be in close proximity to the

CT, trapping the CT between the strait form and the curved form. During a test, raising the bend table forces the CT to conform to the curved form, creating the desired bend radius. Lowering the table forces the CT to conform to the strait form, thus re-straitening the CT. The resulting stress distributions and fatigue implications are discussed in the technical section of this report.

Tension Circuit

Tension is produced in the CT by gripping the CT ends, and pulling on it using two hydraulic pistons. As seen in the diagram below (figure from Autocad), the headstock and tailstock contain the gripping mechanisms described above. The tension is constantly monitored using strain gage type load cells, and an electronic pressure regulator is adjusted based on the load cell signal to produce constant tension. The error between desired and actual tension is constantly monitored and the regulator is controlled to adjust to the error to maintain the desired tension, allowing constant tension to be maintained even during a bend cycle.

Rotation Mechanism

An electric servomotor is connected through a gear reduction to the headstock of the test machine, thus allowing rotation. Rotation can only be achieved while the CT is strait. The motor is controlled via computer or via manual control.

Internal Pressure

The CT can be pressured internally to a pressure of 10,000 psi. A water pump is connected to the headstock. Porting in the headstock directs the fluid into the sealed CT. Manual relief valves are used to remove the internal pressure. Plexiglass shielding protects the operator from the fluid released through a crack in the CT produced at the time of CT failure.

CT Removal and Loading

The tailstock is mounted to an "X" type mechanism coupled to a hydraulic cylinder. It can be raised or lowered. It is also mounted on rollers and bolted into the test machine. By removing these bolts, the entire tailstock mechanism can be pulled back a number of feet. With these two degrees of freedom, CT can be loaded and removed. The first step in the removal process is to remove any internal pressure in the CT. Once this is accomplished, the grips are released, and the tailstock bolts are removed. The tailstock is then pulled back, releasing the CT. The tailstock is lowered, and the CT is removed. The loading sequence is simply the reverse of this process.

ANALYSIS OF CTTM FATIGUE DATA

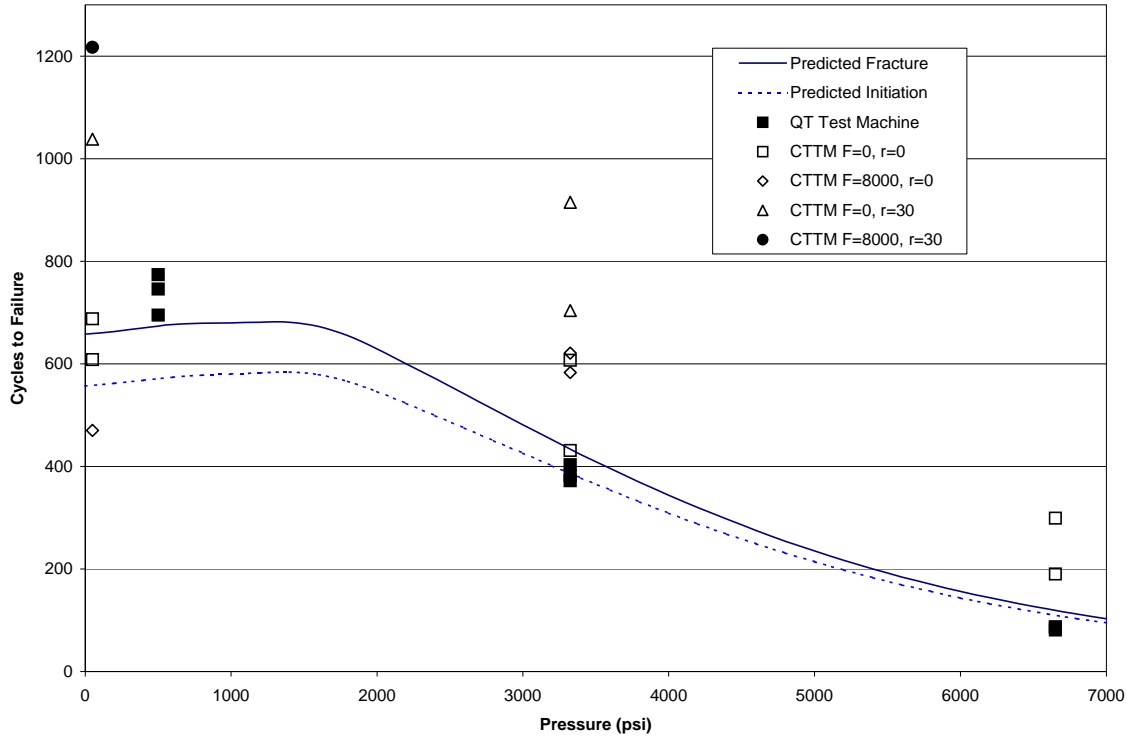


Figure 34
Analysis

Comparison of Fatigue Data from CTES' Coiled Tubing Test Machine & Quality Tubing's Fatigue Test Machine

Data from the CTTM and from a conventional CT fatigue test machine were compared to determine if the CTTM was working correctly. Data from both machines are plotted in Figure 34, along with life predictions made by a commercial software package¹.

Reference data, generated with no axial force or rotation, were generated on the CTTM and on the standard fatigue testing fixture at Quality Tubing. The radius of curvature imposed by each machine is approximately 72 inches. The QT data show good agreement with the predictions. The CTTM data show good agreement with the QT data for the lower pressures, but increasingly longer lives at the medium and higher pressure levels, respectively. At the medium pressure level, the average CTTM life is about 1.3 times the average QT sample life. However, at high pressure, the average CTTM life is 1.88 times the average QT sample life. It is possible that a slightly longer stroke length is needed on the CTTM to achieve a complete wrap of the sample when testing at higher pressures. This will be investigated in future tests.

The preliminary tests involving fatigue cycling with an external axial force of $F = 8000$ lbs. provided mixed results. The single test conducted at low pressure failed in about 72% of the average life of the two samples tested at low pressure without axial force. However, coiled tubing

fatigue lives exhibit considerable scatter at low pressure levels, and this variation is well within a reasonable scatter range. At the medium pressure level, an unexpected result was obtained. The average life from the two samples with an axial force of 8000 lbs. was about 16% longer than the average life of the two baseline tests. This result was surprising, since the 8000 lb. force, combined with the cyclic bending, is predicted to cause significant axial elongation. Measurements taken manually over approximately a 4 inch gauge length showed almost no elongation during the single low pressure test conducted with 8000 lbs., and elongation strains of 0.34% and 0.9% for the two medium pressure tests. Again, more test are required before firm conclusions can be drawn, but it can be said that the axial force appears NOT to increase fatigue damage, relative to cycling without an external axial force, at least for an external axial force up to 10% of the nominal body yield strength.

The tests with rotation shown in Figure 34 show an increase in life, as expected. In the legend in Figure 3, the term “r” represents the rotation in degrees, applied every 3 cycles. Three tests were conducted with no axial force (one at low pressure and two at the medium pressure level) and the life increased by about 60% at low pressure and 56% at medium pressure. This result is not unexpected, since rotating the plane of bending distributes the severe cycling more uniformly over the entire cross section. This increase in life occurs despite the fact that a given portion of the tubing will go from 3 cycles of fully tensile strain to 3 cycles of fully compressive straining, every 18 cycles. The distribution of straining around the cross section appears to offset any increase in fatigue damage caused by doubling of the maximum strain range experienced by a given section of the tubing over its life. This is illustrated in Figure 35, below.

The final, single low-pressure data point of interest is the test conducted with $r = 30$ (30° per 3 cycles) and an axial force of 8000 lbs. This test lasted 17% longer than the rotation test with no axial force, and a factor of 88% longer than the average low-pressure CTTM baseline life. Again the somewhat surprising result is exhibited: a longer life from cycling with axial force than without. Additional tests are needed to confirm the notion that an external axial force enhances fatigue life. At this point, it is possible to state that preliminary tests indicate that external axial force does not *decrease* fatigue life, at least for axial forces up to 10% of the nominal yield strength of the tubing.

The following figure 35 is from a CTES document - Achilles Fatigue Life Prediction Module, from the Cerberus Software Package, CTES, Houston, 1999.

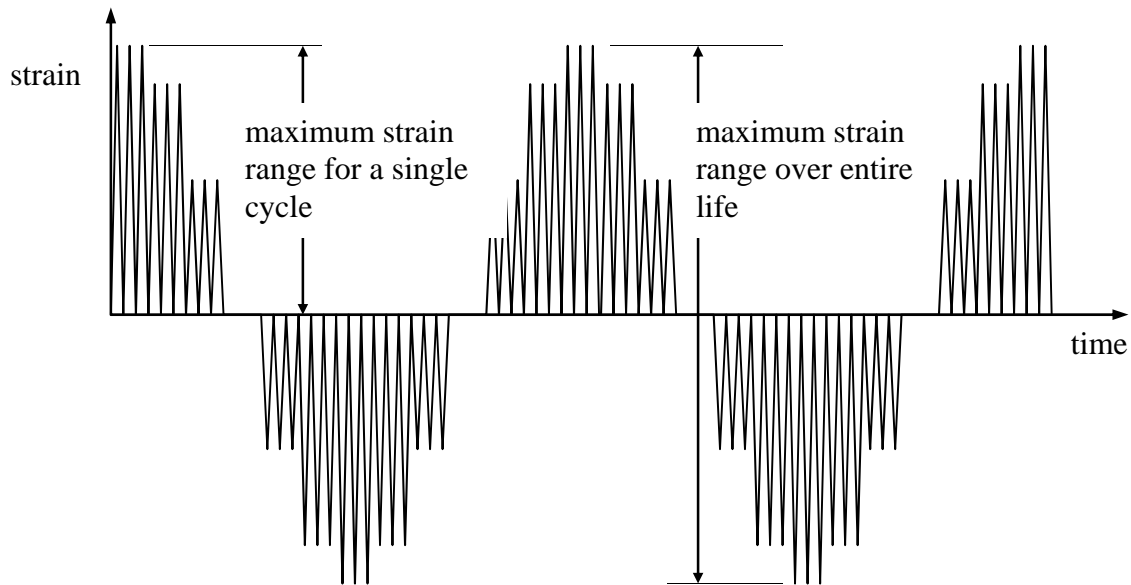


Figure 35 Schematic strain versus time history

Figure 35 above illustrates the schematic strain versus time history for a portion of the cross section during a test involving 30° rotation every 3 trips. Notice how the maximum strain range doubles throughout life, with smaller strain fluctuations in between.

This analysis is limited due to the limited data produced by the CTTM as part of this project.

CONCLUSIONS

The results of cyclic loading experiments and limited theoretical modeling indicate the following:

1. Cyclic loading changes the material properties of CT. The elastic-perfectly-plastic model of material behavior does not apply to CT after the first bend.
2. The yield strength of CT material decreases with increasing strain cycles up to about 20 cycles. In general, the yield stress reduces approximately by 15% during the first 20 cycles.
3. The material property curves exhibit self-similarity when the strain range is in the plastic region. This implies that the family of stress-strain curves for cyclic loading at different strain ranges can be represented by a simple power law.
4. Diametral growth (ballooning of a sample) does not occur without internal pressure. Based on experimental evidence, the relationship between diametral growth and axial strain range appears to be linear.
5. Examination of the role of residual stresses on CT shows that the von Mises criterion (or any incipient yield criterion) does not correctly define operational limit states of CT.
6. Further testing using the CTTM is required to develop an improved limits criteria.

RECOMMENDATIONS

A new approach to defining CT limit states should use LRFD. This would require

1. Rigorous theoretical analysis of CT mechanics,
2. Development of a more complete yield criterion by accounting of residual stresses and changing material properties,
3. Experiments to determine the relationships between loads, resistances, and failures of CT samples,
4. Statistical analysis of experimental data to determine probabilities of failure.
5. Continued testing using the CTTM developed during this project should provide the required statistics.

NOMENCLATURE

Roman symbols

A_o	Area of CT cross section, in ²
c	Capacity or resistance of a structure or member, random variable
d_o	Outer diameter, in
E	Young's modulus, psi
I_o	CT moment of inertia, $= \frac{\pi}{4}(r_o^4 - r_i^4)$, in ⁴
$I_2(y,r)$	Function defined in Equation 5, in ³
$I_3(y,r)$	Function defined in Equation 6, in ⁴
M	Moment, ft-lbs
OD	Outer diameter, in
P	Axial load, lbs
r_o	Outer radius of CT, in
r_i	Inner radius of CT, in
R_b	Bending radius, in
$R_{b,y}$	Yield radius, in
R_n	Nominal resistance of a given parameter
SF	Safety factor
WT	Wall thickness, in
y	Distance from the neutral axis, in

Greek symbols

β	Shift of the neutral plane, in (see footnote # 2)
$\varepsilon ; \varepsilon_y$	Strain; Yield strain
μ	Poisson's ratio
$\sigma ; \sigma_{yp}$	Stress, psi; Yield stress, psi
σ	Stress, psi
σ_a	Axial stress, psi
σ_h	Hoop stress, psi
σ_{rad}	Radial stress, psi
$\sigma_{r,b}$	Residual stress after bend, release, psi
$\sigma_{r,s}$	Residual stress after bend, straighten, release, psi
σ_{vme}	von Mises stress, psi
σ_{yp}	yield stress, psi

Subscripts

b	Bending
s	Straightening
$perm, UL$	Unloading

trans
yp

Transition
Yield point

Other

$||$

Absolute value

$[]$

Interval or region

REFERENCES

- [1] Newman, K., 1991, "Coiled Tubing Pressure and Tension Limits," paper SPE 23131, 1991 Offshore Europe Conference, Aberdeen, Scotland, Sep. 3-6.
- [2] Boresi, A. P., Schmidt, R. J., and Sidebottom, O. M., 1995, *Advanced Mechanics of Materials*, fifth edition, John Wiley and Sons, New York, New York.
- [3] Lubliner, J., 1990, *Plasticity Theory*, Macmillan Publishing Company, New York, New York.
- [4] Lode, W., 1926, "Versuche über den Einfluss der mittleren Hauptspannung auf das Fließen der Metalle Eisen, Kupfer und Nickel," *Z. Phys.* Vol.36, pp 913-919.
- [5] Slater, R. A. C., 1977, *Engineering Plasticity*, John Wiley and Sons, New York, New York.
- [6] Taylor, G. I. And Quinney, H., 1931, "The plastic distortion of metals," *Phil. Trans. R. Soc.*, Vol. A230, pp. 323-62.
- [7] Davis, E. A., 1945, *J. Appl. Mech.*, Vol. 12, p. 13.
- [8] Davis, E. A., 1948, *J. Appl. Mech.*, Vol. 15, p. 216.
- [9] Coffin's paper
- [10] Timoshenko, S., 1975, *Strength of materials, Parts I and II*, reprint edition, Krieger Publishing Company, Malabar, Florida.
- [11] Juvinall, R., 1967, *Stress, Strain and Strength*, McGraw-Hill Publishing Co., New York, New York.
- [12] Sathuvalli, U. B., 1995, "A note on the Permanent Elongation of CT subjected to Bending, Straightening, Axial loading and unloading," Internal Technical Note, CTES, L. C.
- [13] Sathuvalli, U. B., 1996, "Permanent elongation in Coiled Tubing," An internal report submitted to CTES, L. C.
- [14] Newman, K., 1994, PLASTIC , A FORTRAN program to calculate permanent elongation in CT, CTES, L.C., unpublished software, Conroe, Texas.
- [15] Newman, K. 1996, PLASTIC2, revised edition, A FORTRAN program to calculate permanent elongation in CT, CTES, L.C., unpublished software, Conroe, Texas.
- [16] Shah, P. K. and Kyriakides, S., 1985, "Inelastic analysis of thin-walled tubes under cyclic bending," *Int. J. Solids Structures*, Vol. 21, No. 11, pp. 1073-1100.
- [17] Pan, K. and Stelson, S., 1995, "On the plastic deformation of bent tubes," *ASME J. Engg. Ind.*,
- [18] Yang, Y. S., 1996, "Collapse and Burst Pressure of Coiled Tubing Under Axial Load, and Bending Torque and Strain Energy in Spooling CT," paper SPE 36338, 1996 1st SPE-ICoTA North American Coiled Tubing Roundtable, Montgomery, Texas, Feb. 26-29.
- [19] Bhalla, K., 1994, "Implementing residual bend in a tubing forces model," paper SPE 28303, 1994 69th Annual Technical Conference and Exhibition, New Orleans, Sept. 25-28.
- [20] Yeh, W, Cheng, J., and Her, R., 1994, "Analysis of plastic behavior to cyclically uniaxial tests using an endochronic approach," *ASME Journal of Engineering Materials and Technology*, Vol. 116, pp. 62-68.
- [21] Bate, P. S., and Wilson, D. V., 1986, "Analysis of the Bauschinger Effect," *Acta. Metall.*, Vol. 34, pp. 1097-1105.
- [22] Schmidt, L. C. and Morgan, P. R., 1985, " E_T for tensile prestrained tubular struts," *Journal of Structural Engineering*, Vol. 112, pp. 1115-1124.

- [23] Parker, J. and Kettlewell, J., "Plastic stress-strain relationships- Further experiments on the effect of loading history," ASME Journal of Applied Mechanics, Vol. 28, pp. 439-446.
- [24] Schroeder, M., 1991, *Fractals, Chaos, Power Laws*, W. H. Freeman and Co., New York, New York.
- [25] Smythe, W. R. , 1989, *Static and Dynamic Electricity*, 3rd edition, Hemisphere Publishing Corporation, New York, New York.
- [26] Payne, M. L., and Swanson, J. D., 1990, "Application of Probabilistic Reliability Methods to Tubular Designs," *SPE Drilling Engineer*, Dec., pp. 299 - 305.
- [27] Lewis, D. B., Brand, P. R., Whitney, W. S., and Mae, M. A., 1995, 1995, "Load and resistance Factor Design for Oil Country Tubular Goods," OTC paper 7936, presented at the 1995 29th Annual OTC, Houston, May 1 - 4.
- [28] Maes, M. A., Gulati, K. C., McKenna, D. L., Btrand, P. R., Lewis, D. B., and Johnson, R. C., 1995, "Reliability -Based Casing Design," *Journal of Energy Resources Technology*, Vol. 117, pp. 93 - 100.
- [29] Brand, P. R., Whitney, W. S., and Lewis, D. B., 1995, "Load and Resistance Factor Design Case Histories," OTC paper 7937 presented at the 1995 29th Annual OTC, Houston, May 1 - 4.

APPENDIX A: CTTM DESIGN SPECIFICATIONS

DESIGN SPECIFICATIONS FOR: COILED TUBING TEST MACHINE (CTTM) 5/97

- Simultaneously apply tension, bending and internal pressure
 - Tension *with* bending event: 10,000#
 - Tension *only*: 200,000#
 - Internal pressure capability: 10,000 PSI
 - Bending capability: 3.5" O.D. x 0.25" W.T. CT @ 100,000 min yield.
Bend form has sufficient movement to engage CT sample a minimum of 10 diameters.
 - Bend forms radii: 48" for 1.25" and 1.50" CT
72" for 1.75" through 2.38" CT
100" for 2.88" through 3.50" CT
 - Tubing sizes: 1.25" O.D. through 3.50" O.D.; all wall thicknesses
 - Ability to index CT sample *between* any event. Indexing accuracy is ± 0.25 degrees. Nominal minimum indexing increment is 10 degrees of rotation.
 - Qualitative requirements;
 1. Short, manageable CT samples; 109" long.
 2. Automatic or manual cycling capability
 3. Skid mounted
 4. One-man operation
 5. No welding on CT sample (for end connection attachment)
 6. Use load cells to precisely measure/record tension loads
 7. Use pressure transducers to precisely measure/record pressures
 - Measurements to be taken;
 - A. Tension during bending
 - B. Tension without bending
 - C. Internal pressure
 - D. Elongation extensometer
 - E. Hydraulic pressures
 - F. Index position (orientation)
 - G. Bend event hydraulic cylinder position (with LVDT and inductive proximity switch)
 - H. Bend "straightener" position to prevent reverse bending during straightening of the CT sample (with inductive proximity switch)
- Note: All measurements will be monitored with the CTES Orion data acquisition system.

APPENDIX B: SURGE TANK CALCULATIONS

If the volume of a pressurized vessel is changes, the pressure exerted by the fluid in the vessel changes. The change in pressure ΔP for a volume change ΔV is given by

$$\text{Equation B 1} \quad \Delta P = -\frac{\Delta V}{V_o} E_b$$

where E_b is the bulk modulus of the pressurizing liquid. The change in the volume corresponds to the change in the dimensions of the vessel. In this case, the vessel is the CST test specimen.

Lame's equations (Boresi et al., 1995) describe the stresses and strains in cylindrical vessel subjected to internal and external pressures. The radial, circumferential and axial stresses in a closed cylindrical enclosure subjected to an internal pressure p_i and axial load P are given by

$$\text{Equation B 2} \quad \sigma_{rad}(r) = \left(1 - \frac{r_i^2}{r^2}\right) \frac{p_i r_i^2}{r_o^2 - r_i^2} - \frac{p_i r_i^2}{r^2}$$

$$\text{Equation B 3} \quad \sigma_{hoop}(r) = \left(1 + \frac{r_i^2}{r^2}\right) \frac{p_i r_i^2}{r_o^2 - r_i^2} + \frac{p_i r_i^2}{r^2}$$

and

$$\text{Equation B 4} \quad \sigma_{axial} = \frac{p_i r_i^2}{r_o^2 - r_i^2} + \frac{P}{\pi(r_o^2 - r_i^2)}$$

where r is the distance of a point from the axis of the cylinder, and r_o and r_i denote the outer and inner radii respectively. The corresponding strains are given by

$$\text{Equation B 5} \quad \varepsilon_{rad}(r) = \frac{1}{E} \left[\sigma_{rad}(r) - \mu(\sigma_{hoop}(r) + \sigma_{axial}) \right]$$

$$\text{Equation B 6} \quad \varepsilon_{hoop}(r) = \frac{1}{E} \left[\sigma_{hoop}(r) - \mu(\sigma_{rad}(r) + \sigma_{axial}) \right]$$

and

$$\text{Equation B 7} \quad \varepsilon_{axial} = \frac{1}{E} \left[\sigma_{axial} - \mu(\sigma_{rad}(r) + \sigma_{hoop}(r)) \right].$$

Note that the radial and hoop quantities are functions of the radius and vary across the cross section. The change in the outer and inner radii for a given axial strain ε_z can be shown to be

Equation B 8

$$\Delta r_o = r_o \left[\frac{1-2\mu}{A_o E} p_i A_{in} + (1+\mu) \frac{A_{in}}{A_o E} p_i - \mu \varepsilon_{axial} \right]$$

and

Equation B 9

$$\Delta r_i = r_i \left[\frac{1-2\mu}{A_o E} p_i A_m + (1+\mu) \frac{A_{out}}{A_o E} p_i - \mu \varepsilon_{axial} \right]$$

respectively. The change in length of the cylinder is

Equation B 10

$$\Delta L = L \varepsilon_{axial}$$

where L is the original length of the cylinder. The change in volume can now be computed and used to calculate the corresponding change in pressure from Equation B 1. Consider a 1.5” x 0.109” 3” long CT test specimen made of 70 ksi material. Let the internal pressure be 2000 psi. If this specimen is subjected to seven times the yield strain in the axial direction, the volume change would increase the pressure by approximately 107%. Therefore, a surge tank must be provided as shown in Figure B 1.

Let the volume of the surge tank be V_{surge} . Then the change in pressure due to a change in volume ΔV of the test specimen is

$$\Delta P = -\frac{\Delta V}{V_{test} + V_{surge}} E_b$$

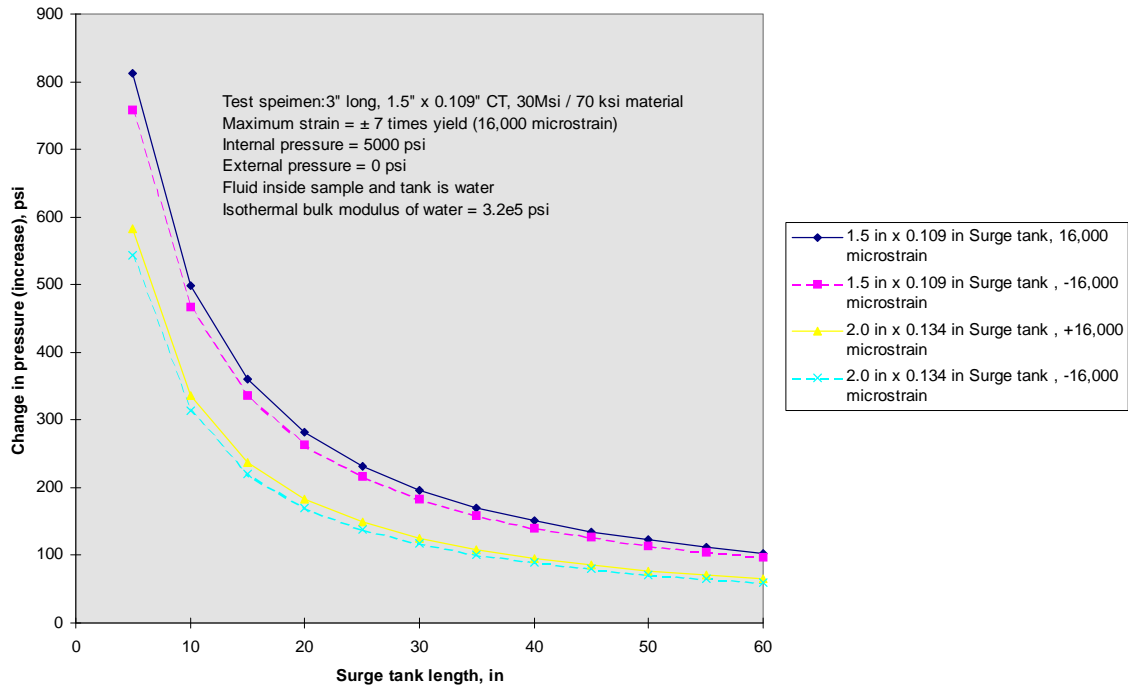


Figure B 1 Surge tank length versus change in pressure

If $V_{surge} \gg V_{test}$ the change in the test specimen pressure is acceptably small.

Let the surge tank be a thick walled cylindrical vessel with closed ends. Figure B 1 shows the percentage change in pressure due to volume change caused by axial strain (of \pm seven times nominal yield strain) as a function of the length of the surge tank, for two different sizes of OD and wall thickness. In both cases, the magnitude of the pressure change decreases hyperbolically with surge tank length. Based on the curves shown in Figure B 1, we chose a 2.375" x 0.109" CT sample that was 60" long. Suitable end pieces were welded at either end of the sample.

APPENDIX C LOG OF CST 1-8

CST 1: Half range test without internal pressure

Date:	January 2, 1996, 8.25 A. M
Place	Civil Engineering Department, Rice University
Nominal size:	1.5" x 0.109"
Length of specimen	3"
Nominal yield strength	70,000 psi
Measured yield strength	75,245 psi
Internal pressure	0 psi
Strain range	16,500 to -16,500 $\mu\epsilon$
Total number of cycles	100
Transducers	Load cell, Axial extensometer
Data Acquisition	Load cell and extensometer readings were updated by the Rice University Data Acquisition System.
Frequency of cycling:	
Cycles 1 to2	Manual, strain versus time is a ramp of slope 1 thousand-strain per second
Cycles 3-25	strain versus time is triangular waveform of 0.01 Hz
Cycles 26 - 100	0.1 Hz

Notes:

- The test was interrupted after 25 cycles because the INSTRON machine developed a problem and could not be used. The sample was unloaded when the axial strain in the sample was at tensile stress and zero strain. The residual strain in the sample was noted to be -2905 microstrain (compressive).
- The test was resumed on January 5, 1996 after the machine was fixed. The sample was first loaded in tension till it reached a strain of 2905 microstrain. The extensometer was then reset to read zero strain at this point. Cycle # 26 was counted from this point onwards.
- The extensometer was fastened to the sample by means of rubber bands. After 50 cycles, the sample developed ridges in the rubber band planes. These ridges were visible to the naked eye.
- After 100 cycles, the sample developed a longitudinal crack near the weld between the sample and the upper adapter. The test was stopped at this stage.

CST 2: Half range tension test without internal pressure

Date	January 5, 1996, 11.00 A. M
Place	Civil Engineering Department, Rice University
Nominal size	1.5" x 0.109"
Length of specimen	3"
Nominal yield strength	70,000 psi
Measured yield strength	75,245 psi
Internal pressure	0 psi
Strain range	16,500 to 0 $\mu\epsilon$
Total number of cycles	100
Transducers	Load cell, Axial extensometer
Data Acquisition	Load cell and extensometer readings were updated by the Rice University Data Acquisition System.
Frequency of cycling:	
Cycles 1 to2	Manual, strain versus time is a ramp of slope 1 thousand-strain per second
Cycles 3-25	strain versus time is triangular waveform of 0.01 Hz
Cycles 26 - 100	0.1 Hz

CST 3: Half range compression test without internal pressure

Date: January 5, 1996, 1.40 P. M
Place: Civil Engineering Department, Rice University
Nominal size: 1.5" x 0.109"
Length of specimen 3"
Nominal yield strength 70,000 psi
Measured yield strength 75,245 psi
Internal pressure 0 psi
Strain range 0 to -16,500 $\mu\epsilon$
Total number of cycles 100
Transducers Load cell, Axial extensometer
Data Acquisition Load cell and extensometer readings were updated by the Rice University Data Acquisition System.

Frequency of cycling:
Cycles 1 to2 Manual, strain versus time is a ramp of slope 1 thousand-strain per second
Cycles 3-25 strain versus time is triangular waveform of 0.01 Hz
Cycles 26 - 100 0.1 Hz

CST 4: Test failed

Date:	June 11, 1996, 2:00 P. M
Place	Civil Engineering Department, Rice University
Nominal size:	1.5" x 0.109"
Length of specimen	3"
Nominal yield strength	70,000 psi
Measured yield strength	71,500 psi
Internal pressure	2000 psi
Strain range	N/A
Total number of cycles	N/A
Transducers	Load cell, Pressure cell, Axial extensometer, Hoop strain gage
Data Acquisition	N/A. This test was used to debug the CTES Acquisition System.
Frequency of cycling:	N/A

Notes:

- After the voltage attenuator shown in Fig. 1 was incorporated across channels 1 and 2 of the SC-2070 board, the experiment was started.
- However, we noticed that the axial strain as read by LABVIEW and our DAQ did not match the reading on the INSTRON control panel. By this time, the sample had already yielded. We know this because the load had exceeded 33000 lbs and Dr Merwyn's DAQ system was recording a straight (load versus axial strain) line.
- We brought the load back to zero and re-calibrated the extensometer, and ensured that the readings on our system matched the readings on Dr Merwyn's system.
- We then compressed the sample to zero strain. When we tried to compress it further to a strain of $-16500 \mu\epsilon$, we noticed that the stroke length on the machine was insufficient. The test specimen had been mounted in the loading frame such that we could not reach the goal of $-16500 \mu\epsilon$.
- Furthermore, while calibrating the extensometer, we had to load and unload the sample.
- These operations had loaded the sample well beyond the plastic range and we decided to scrap the sample and stop testing on it.
- We noted that the hoop strain as read by the LABVIEW and the strain as read by the p-3500 strain indicator differed by $60 \mu\epsilon$ throughout. (We observed this during all the tests). Therefore, we must correct all the hoop strains in the data files according to the following relation: Actual hoop strain = hoop strain in data file + 60 .
- The above relation is valid when all strains are expressed in microstrain.
- Since the INSTRON controller reads strain in thousand strain, we made our data acquisition system read the axial strain in the same units. Therefore, multiply all axial strain values in the raw data by 10^3 to obtain the microstrain.
- All data files can be open as spreadsheets. The data is stored in 4 columns as follows:

Column 1	load, lbs	Column 3	Hoop strain, microstrain
Column 2	Pressure, psi	Column 4	Axial strain, thousand strain
- Test # 4 thus served only to debug the procedure and the data acquisition system.

CST 5 Full range test at 2000 psi internal pressure:

Date:	June 11, 1996, 4:00 P. M
Place	Civil Engineering Department, Rice University
Nominal size:	1.5" x 0.109"
Length of specimen	3"
Nominal yield strength	70,000 psi
Measured yield strength	72,000 psi
Internal pressure	2000 psi
Strain range	16,500 to -16,500 $\mu\epsilon$
Total number of cycles	10
Transducers	Load cell, Pressure cell, Axial extensometer, Hoop strain gage
Data Acquisition	The readings were updated by the CTES Data Acquisition System as follows. Every 125 ms, each of the 4 channels was sampled to obtain 100 samples at 10,000 samples per second. The average of these 100 samples was recorded.
Frequency of cycling:	0.01 Hz

Notes:

- By the end of 7 cycles, the sample had ballooned noticeably and resembled a pair of bellows. It seemed that failure was imminent. Moreover, the hoop strain gage was not working by this time. I believe it may have failed after 7 cycles (must confirm this by checking the data file).
- Because of the ballooning and bellows effect, we decided to stop the test. These two effects would render the axial strain data meaningless. The extensometer blades were no longer in contact with a plane surface and the gage length was not 1".
- We did not observe any heating of the sample.
- The pressure remained more less steady at 2000 psi. A variation of ± 50 to 100 psi was seen.
- After the cycling^{*}, we brought the load back to zero. We reset the extensometer to zero strain and performed a pull test to 5% strain. The data was recorded. The pull test however, smoothed out the bellows-shape that the sample had assumed after cycling.

^{*} End of a cycle is at zero strain and finite tensile load (approx. the yield load ignoring Bauschinger effect).

CST 6: Half range tension test at 2000 psi internal pressure

Date:	June 12, 1996, 8:30 A. M
Place	Civil Engineering Department, Rice University
Nominal size:	1.5" x 0.109"
Length of specimen	3"
Nominal yield strength	70,000 psi
Measured yield strength	72,000 psi
Internal pressure	2000 psi
Strain range	16,500 to 0 $\mu\epsilon$
Total number of cycles	100
Transducers	Load cell, Pressure cell, Axial extensometer, Hoop strain gage
Data Acquisition	The readings were updated as follows. Every 62.5 ms, each of the 4 channels was sampled to obtain 500 samples at 10,000 samples per second. The average of these 500 samples was recorded in the data file.
Frequency of cycling	
Cycles 1 to 3	Manual, strain versus time is a ramp of slope 1 thousand-strain per second
Cycles 3-12	strain versus time is triangular waveform of 0.01 Hz
Cycles 13 - 22	0.01 Hz
Cycles 23-31	0.1 Hz
Cycles 32 - 100	0.1 Hz

Notes:

- The bellows effect was not significant, at least not noticeable with the naked eye.
- The ballooning was not noticeable either.
- The hoop gage lasted all the 100 cycles.

CST 7: Full range test without internal pressure

Date:	June 12, 1996, :10.00 A. M
Place	Civil Engineering Department, Rice University
Nominal size:	2.0" x 0.134"
Length of specimen	3"
Nominal yield strength	70,000 psi
Measured yield strength	75,000 psi
Internal pressure	0 psi
Strain range	6000 to -6000 $\mu\epsilon$
Total number of cycles	100
Transducers	Load cell, Pressure cell, Axial extensometer, Hoop strain gage
Data Acquisition	The readings were updated as follows. Every 62.5 ms, each of the 4 channels was sampled to obtain 500 samples at 5,000 samples per second. The average of these 100 samples was recorded in the data file.
Frequency of cycling:	
Cycles 1 to 5	strain versus time is a ramp of slope 1 thousand-strain per second
Cycles 5 - 100	strain versus time is triangular waveform of 0.1 Hz

Notes:

- The clearance between the 2" sample and the collar (whose diameter is 2.1") was insufficient to accommodate the gage wires. Therefore, the strain gage lead wires were soldered on to the gage terminals after the sample was inserted in to collar.
- The INSTRON loading machine has a capacity of approximately 56 kips. The expected yield load of this sample was 58.9 kips.
- We wanted to cycle the sample between $\pm 14,000 \mu\epsilon$. We first loaded the sample in tension and yielded it to 14,000 $\mu\epsilon$. We then unloaded the sample and compressed it to zero strain. We could not push the machine to compress the sample to -14,000 $\mu\epsilon$. The machine stalled at -7,700 $\mu\epsilon$. In short we could not achieve the desired strain limits of cycling and settled down finally to cycling between $\pm 6,000 \mu\epsilon$. The following is the loading sequence:

Cycle 1:	0 to 14,000 $\mu\epsilon$, 14,000 $\mu\epsilon$.to 0, 0 to -7,700 $\mu\epsilon$, -7,700 $\mu\epsilon$ to 0
Cycle 2	0 to 12,600 $\mu\epsilon$, 12,000 $\mu\epsilon$ to 0, 0 to -6700 $\mu\epsilon$, -6,700 $\mu\epsilon$ to 0
Cycle 3 -100	0 to 6000 $\mu\epsilon$, 6000 $\mu\epsilon$ to 0, 0 to -6000 $\mu\epsilon$, -6000 $\mu\epsilon$ to 0

CST 8: Full range tension test at 2000 psi internal pressure

Date:	June 12, 1996, :12.00 noon
Place	Civil Engineering Department, Rice University
Nominal size:	2.0" x 0.134"
Length of specimen	3"
Nominal yield strength	70,000 psi
Measured yield strength	75,000 psi
Internal pressure	2000 psi
Strain range	6000 to -6000 $\mu\epsilon$
Total number of cycles	75
Transducers	Load cell, Pressure cell, Axial extensometer, Hoop strain gage
Data Acquisition	The readings were updated as follows. Every 62.5 ms, each of the 4 channels was sampled to obtain 500 samples at 5,000 samples per second. The average of these 100 samples was recorded in the data file.
Frequency of cycling	
Cycle 1 to 3	strain versus time is a ramp of slope 1 thousand-strain per second
Cycle 4 -75	strain versus time is triangular waveform of 0.05 Hz

Notes:

- The clearance between the 2" sample and the collar (whose diameter is 2.1") was insufficient to accommodate the gage wires. Therefore, the strain gage lead wires were soldered on to the gage terminals after the sample was inserted in to collar.
- In the light of the events of test 7, we decided to cycle the specimen between 6000 to -6000 $\mu\epsilon$.
- The pressure kept falling and had to be bumped every few minutes.
- Hoop gage failed at about the 56th cycle. We stopped the test after the 75th cycle.
- The bellows-effect was absent.
- The ballooning was visible to the naked eye.
- There was no heating of the sample.
- After the specimen was unscrewed from the loading frame, it could not be removed from the collar. The diameter of the collar was lesser than the ballooned diameter of the specimen.